Workability Analysis of a Floating XL-Monopile Installation

A vessel motion study

J.M. (Job) Bottemanne

October 2020

TU Delft

Workability Analysis of a Floating XL-Monopile Installation

A vessel motion study

by

J.M. (Job) Bottemanne

to obtain the degree of Master of Science
at the Delft University of Technology,
to be defended publicly on Thursday, October 1st, 2020 at 14:30 PM

Master Programme:	Offshore & Dredging Engineering	
Student number:	4211200	
Project duration:	September 2019 – October 2020	
Thesis committee:	ir. A.C.M. van der Stap,	TU Delft, chairman
	ir. P. van der Male,	TU Delft, daily supervisor
	Dr. ir. K.N. van Dalen,	TU Delft, committee member
	ir. K. van der Heiden,	Jumbo Maritime, supervisor

This thesis is confidential and cannot be made public until October 1st, 2025

An electronic version of this thesis is available at `http://repository.tudelft.nl/`.

TU Delft

JUMBO

Preface

After years of studying, this thesis is the final work done to obtain a masters degree in Offshore & Dredging Engineering at Delft University of Technology.

My gratitude goes out to Jumbo Maritime for giving me the opportunity to perform research on a very interesting topic in the field of Offshore Engineering. I have truly enjoyed being in their beautiful office in Schiedam with an amazing view over the river where the Jumbo vessels regularly pass by.

Next, my sincerest appreciation goes to Kasper van der Heiden, supervisor from Jumbo Maritime. He guided me through this intense learning period by always being there to discuss my assumptions or my doubts. Due to his dedication and advice, this learning period was not only educational but also very enjoyable.

I would also like to thank my daily supervisor, Pim van der Male, and the chairman of my committee, Andre van der Stap, for providing me with the tools, support and critical notes to be able to conduct this research.

Furthermore, I would like to thank my fellow graduate students at Jumbo Maritime, Niels van Duijn, Michiel Bicker and Niek Hagen for always being available to discuss the problems I was facing. The same goes for Jelle Teeling, Martijn van Gils, Roland Martens and Thomas Taks. The discussions about each others research, although the topics were different, really made it possible to put a lot of the problems I was facing into perspective.

Lastly, I want to thank my family and friends for always supporting me during this sometimes challenging period.

J.M. (Job) Bottemanne
Delft, October 2020

Abstract

In order to meet the climate goals to minimize the global temperature rise, an accelerated growth of renewable energy sources is necessary. Within the renewables market, the offshore wind sector takes a big part and has experienced a rapid growth over the past years. Around 80% of offshore wind turbines have a monopile foundation, (a large diameter tubular support structure). In present time, monopiles are installed by using either a jack-up or a floating vessel. Due to the trend in the offshore industry that wind turbines increase in size and that wind locations move to deeper waters, an installation with floating vessels may become the most cost-effective option.

Jumbo Maritime has designed a new vessel to expand its offshore fleet: HLCV Stella Synergy. This heavy lift crane vessel will be used to install monopiles. Multiple installation methods are under consideration and this thesis focuses on the method with mooring lines to provide station-keeping during the installation. Due to the footprint of the vessel relative to an earth-fixed position, a motion compensated pile gripper is used to maintain upright position of the monopile.

During the early driving phase (see Figure 1) of the installation, the monopile has limited interaction with the soil and acts as an unstable inverted pendulum. The upright position of the monopile is maintained by the gripper frame. The forces applied by the gripper frame on the monopile are reaction forces on the vessel. These reaction forces on the vessel can cause an increased vessel footprint. A workability assessment is performed for a moored floating monopile installation, and the influence of the gripper frame reaction forces on this workability is analyzed.

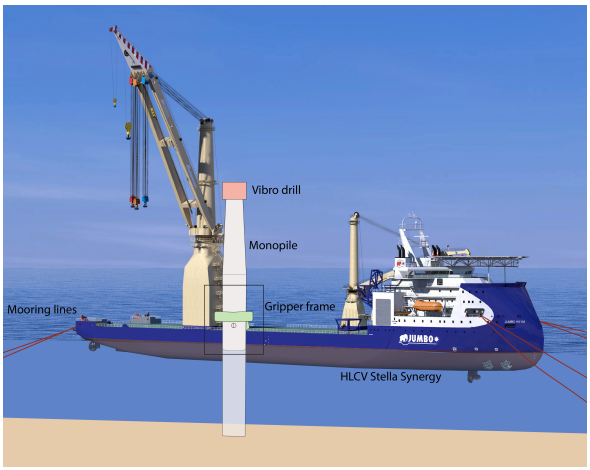

Figure 1: Early driving phase of a monopile installation

Considering nonlinear phenomena in the installation system, such as a gripper frame control system and viscous drag forces, a time-domain simulation model is made in AnySim XMF for which a hydrodynamic database is used as input. The provided hydrodynamic database is based on the results of a scale model test in a water basin, for one specific loading condition. The provided hydrodynamic database is also compared with an AQWA calculation. The reaction forces from the gripper frame are determined with a MATLAB/Simulink model which generates a gripper force time series based on the behavior of the monopile and the gripper frame due to environmental loading. This gripper force time series is applied to the vessel as an external force during the time-domain simulations. During these 3 hour simulations, the vessel is subjected to co-linear environmental conditions from two different incoming directions, while the vessel is moored to the seabed. The workability is calculated for sea conditions in the North Sea. In a second simulation model, the same simulations are performed but without the gripper frame force time series applied to the vessel to determine its influence on the total workability of the installation.

The gripper frame forces have no significant influence on the workability of a monopile installation. In beam waves, the workability is limited by excessive roll motions for longer waves and by insufficient station-keeping from the mooring lines for higher waves. The loading condition addressed in this research proves unfavorable due to its low roll natural frequency. Investigation is needed whether this loading condition is representative of a loading condition which is likely to occur during a monopile installation. In head waves, the system performs satisfactory and is mildly limited by excessive roll and pitch motions.

List of Symbols and Abbreviations

Abbreviations

CoG	Center of Gravity
DOF	Degree of Freedom
DP	Dynamic Positioning
HLCV	Heavy Lift Crane Vessel
HMPE	High Modulus Polyethylene
ILT	Internal Lifting Tool
MBL	Minimum Breaking Load
PID	Proportional-Integral-Derivative
QTF	Quadratic Transfer Function
RAO	Response Amplitude Operator

Symbols

μ	Incoming wave direction
Φ_0	Undisturbed wave potential
Φ_7	Diffraction potential
ρ	density
ζ_a	Wave amplitude
g	Gravitation constant
I	Moment of inertia
S_ζ	Wave spectrum
$S_{JONSWAP}$	JONSWAP spectrum
S_u	Motion spectrum

List of Figures

List of Tables

Contents

1 Introduction

This Chapter introduces the reader to the subject and explain the relevance of this research. First, background information on the current development of offshore wind foundation installation is given, followed by a description of the problem, a research question and an approach to how an answer to the research question can be found.

1.1. Background information

This section gives background information on the development of Offshore Wind Turbines and explains the relevance of this research.

To limit the effects of global warming, the Paris Agreement was put to life in 2015. This agreement brings all nations to a common cause to undertake ambitious actions to combat climate change. Its central goal is to keep the global temperature rise below 2 degrees Celsius above pre-industrial levels and to pursue efforts to limit the temperature increase even further to 1.5 degrees Celsius[United Nations, 1992]. The United Nations state that to meet the Paris Agreement climate goals on time, an accelerated growth of renewable energy sources such as wind and solar is necessary.
The targets implied by the Paris Agreement demand 150 GW of offshore wind capacity in the North Sea to be installed by 2040. The installed capacity in the North Sea is currently 17 GW and the deployment rate is approximately 2 GW/year while an average deployment rate of 7 GW/year over the period 2023-2040 is required to reach the Paris Agreement target [North Sea Wind Power Hub, 2019]. Clearly an increase in deployment rate is necessary and to make this happen the offshore industry will have to pursue a cost decrease on all cost components of the turbine and its foundation. One clear trend in the offshore industry to decrease costs is that wind turbines to be installed get larger in size and capacity every generation. The next generation wind turbine, the 12 MW GE haliade-X, will be 260m tall and have rotor blades of 107m long [General Electric, 2019]. When this giant structure is installed, its height above the water level is almost as high as the Eiffel Tower in Paris. One can imagine that such a structure requires a very large foundation as well. The bottom founded offshore wind support structures that are currently used in the industry are depicted in Figure 1.1. To put it in perspective: to support this new 12 MW GE Haliade-X, a monopile would be needed with a diameter of around 10m. This monopile, depending on site specific soil conditions and water depth, can weigh up to 2200 tonnes [Buitendijk, 2016] and can also be classified as an Extra Large Monopile (XL-Monopile).

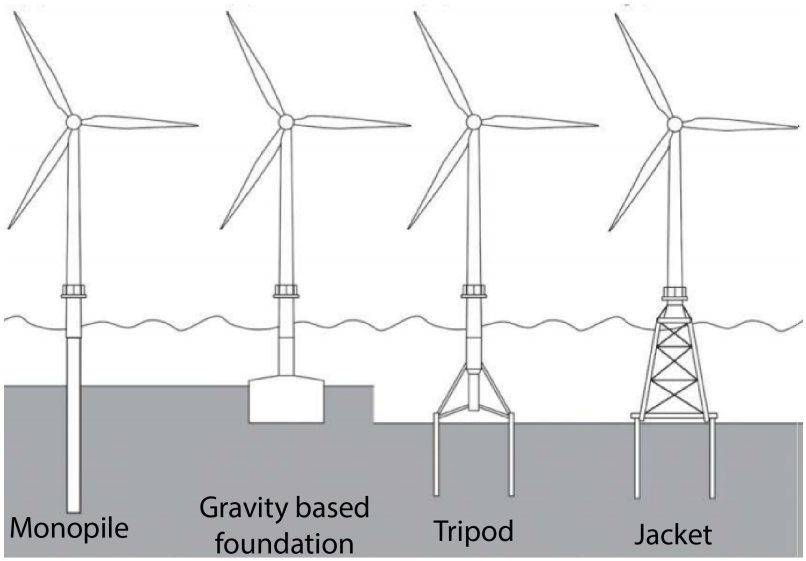

Figure 1.1: Existing wind turbine foundations [Male, 2018]

Out of all offshore wind turbines installed in the North Sea in 2019, 80% have a monopile foundation and it is expected that the monopile will remain the most preferred foundation type for turbine installations in the coming years, even in water depths of up to 40 meters and turbines increasing in size [WindEurope, 2019]. The monopile owes this preference to its proven track record and its manufacturing simplicity compared to jackets, tripods and gravity based foundations. Because the monopile takes a major part of the applied foundations at this moment in time, it is therefore subject of this research. This thesis investigates a monopile installation method with the aim to decrease installation costs.

Jumbo Maritime

Jumbo Maritime is a heavy lift shipping and offshore transportation & installation contractor and will soon add a new vessel to the fleet: Heavy Lift Crane Vessel (HLCV) Stella Synergy. This multi-purpose offshore installation vessel with dynamic positioning system (class DP2) will service the global offshore energy industry by installing wind turbine foundations, oil & gas facilities and subsea infrastructure. It is equipped with a main crane with a maximum lifting capacity of 2500 tonnes and an auxiliary crane with a capacity of 400 tonnes.

Figure 1.2: Render of HLCV Stella Synergy [Jumbo, 2019]

HLCV Stella Synergy will be capable of installing these large monopiles, and Jumbo desires the vessel to be able to install monopiles with sizes ranging from 6 to 11 meters in diameter and weights of up to 2500 tonnes. The method to install these large monopiles with HLCV Stella Synergy is addressed in this research.

1.2. Monopile installation

This section provides the reader with an introduction to the systems used during a monopile installation, and currently used work methods and a typical installation sequence are discussed. Before these installation methods are described, it is important to underline the meaning of workability. The workability of an installation is the percentage of time in a year that the vessel is able to perform the installation at a specific location. If it is possible to install a monopile under rougher environmental conditions, the vessel can work more days in a year and thus perform more installations in a year. Every installation method has its limitations i.e. maximum allowable wave conditions below which it is safe to perform the installation.

Installation methods

Monopile installations are typically performed by using a heavy lift crane vessel. The monopile is transported, lying horizontally, on deck. On site, the monopiles are lifted to a vertical position, which is called upending. Next, the monopile is positioned into a monopile gripper frame, which holds the monopile in an upright position while it is driven into the seabed. This gripper frame can either be fixed to the installation vessel, or a motion compensated gripper frame can be used. This motion compensated gripper frame controls the position of the monopile relative to the vessel and it is able to maintain an earth fixed position for the monopile while connected to a moving vessel. An example of a motion compensated pile gripper frame can be seen in Figure 1.3. A typical gripper frame has a dynamic part that controls the (horizontal) position of the monopile relative to the vessel i.e. this dynamic part is able to maintain an earth-fixed position while connected to a moving vessel. In Figure 1.3 this dynamic part of the gripper frame consists of a supporting ring, which is connected to the monopile by applying pressure with its arms. This supporting ring is able to move horizontally relative to the vessel by sliding across the supporting beams.

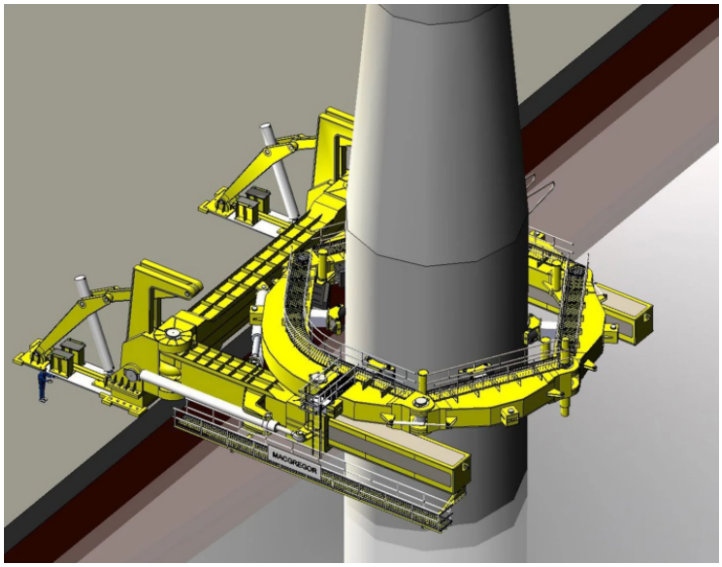

Figure 1.3: Example of a motion compensated pile gripper [MacGregor,2018]

In the past, monopile installations were carried out by two different types of vessels: jack-up vessels and moored floating vessels.

Figure 1.4: Seajacks Scylla installing a monopile [Seajacks, 2018]

Figure 1.5: Oleg Strashnov installing a monopile [Seaway Heavy Lifting, 2015]

Jack-up vessel:
A Jack-up vessel has the capability of jacking up the whole vessel above the water with its legs. Standing on these legs, the vessel is almost completely motionless and is barely influenced by environmental conditions during the installation. In this stable configuration the vessel is able to install monopiles with high accuracy in terms of vertical inclination. Also the rotation of the monopile around its longitudinal axis can be controlled, for the wiring holes need to face a certain direction. The downside of using a jack-up vessel is the fact that jacking up the vessel takes a considerable amount of time. The jacking duration is in the same order as the time needed for pile driving [Buitendijk, 2016]. The soil conditions also play an important role for a jack-up vessel as these affect the vessel's stability when it is standing on its legs. Finally, the water depth is of importance for a jack-up vessel. The maximum water depth is limited by the length of the legs, and the maximum lifting capacity decreases with increasing water depth to remain in a stable configuration. In Figure 1.4 one of the largest Jack-up vessels, the Seajacks Scylla, is displayed installing a monopile by using a fixed pile gripper frame.

Moored floating vessel
Moored floating vessels are also used for monopile installations. The benefit of using a floating vessel is the fact that the soil conditions do not influence the lifting stability, as it is not standing on the soil. The mooring lines keep the vessel stationary relative to an earth fixed location. A vessel can be moored by either a catenary mooring system or a taut leg mooring system. In a catenary mooring system, the restoring force is generated by the weight of the mooring line. In a taut leg mooring system this restoring force is generated by the elasticity of the mooring lines.

For both mooring systems the vessel will have a footprint around its set position in the horizontal plane. The size of this footprint depends on the environmental conditions, the number of mooring lines, the mass of the mooring lines and the pretension in the mooring lines [Nejad et al., 2018]. The workability for the installation from a moored floating vessel is relatively small, as the vessel motions are limiting the operation. This workability can be increased by using a motion compensated pile gripper instead of a fixed pile gripper frame. This gripper frame compensates the vessel motions and reduces the induced monopile motions. This allows for larger vessel motions to perform the installation. In Figure 1.5 the Oleg Strashnov can be seen installing a monopile using a motion compensated pile gripper frame.

DP-controlled floating vessel
A proposed monopile installation method is the installation from a floating vessel which performs its station-keeping with the use of its Dynamic Positioning (DP) system. A DP-system maintains a set position, heading or course by making use of its thrusters to counteract environmental forces. A DP-vessel, the same as with the moored floating vessel installation method, will also have a footprint around its set earth-fixed position due to the time-varying environmental forces acting on the vessel.

The size of this footprint depends on the DP-capabilities of the vessel. For this method also a motion compensated pile gripper is needed. The size of the gripper envelope is directly related to the vessel footprint, as it compensates the vessel motions when it drifts from its set position.

This research focuses on a monopile installation with a floating vessel, thus a jack-up vessel is not considered. The floating vessel used throughout this thesis is based on HLCV Stella Synergy.

1.2.1. Floating installation sequence

The following phases in a monopile installation from a floating vessel can be distinguished:

1. **Monopile transport**
   The monopile is transported to the installation site. This can be done in multiple ways. The monopile can be transported on deck of the installation vessel but it can also be transported on a barge after which it is lifted to the deck of the installation vessel. Another method is to let the monopile float by attaching end caps. It is then towed to the installation site by a tug. Arriving on location, the installation vessel deploys its moorings or activates its DP-system.

2. **Monopile upending**
   The monopile is transported horizontally. Multiple methods of upending are being used. If a monopile is transported floating in the water, it is upended by attaching the crane of the installation vessel to one end of the monopile, by using an Internal Lifting Tool (ILT), and lifting it upwards. Using this upending in water technique requires a controlled de-ballasting of the monopile for otherwise the crane can get overloaded. To upend a monopile when it is laying on deck mostly an upending tool is used consisting of a hinge and a shoe in which the monopile stands after the upending process. In Figure 1.6 an upended monopile is visualized. The work of [Veen, 2019] describes the difficulties and risks that are encountered during the upending process.

3. **Lowering of monopile to the seabed**
   After the upending process, the monopile is released from the upending tool by lifting it out of the upending shoe and is freely hanging below the main crane. To be able to suspend such a large sized monopile alongside the vessel, the crane tip reaches very high which is not favorable for the vessel's stability. The monopile also experiences wave and current loading for it is partly submerged. Positioning the monopile into the gripper cannot be performed under all circumstances as unwanted monopile movement can limit the operation. When the monopile is positioned in the gripper, it is lowered through the splash zone and set on the seabed. During this lowering, the monopile experiences loading from waves, wind and current.

4. **Early driving phase**
   The monopile penetrates the seabed upon touchdown due to its own weight. The self penetration depth depends on the soil properties and the monopile dimensions. The exact location where the monopile touches the soil in the horizontal plane is now determined, and the gripper frame is activated to maintain upright position of the monopile above this set location. Now the ILT is detached from the monopile which is an important decision point in the installation process. If weather conditions would deteriorate towards unacceptable limits after this point, the activity to abort the operation and re-attach the ILT, hoist the monopile back out of the water and prepare for commute back to shore is quite complicated and more time-consuming than before detaching the ILT. Also note that from this point it is crucial for the gripper frame to maintain upright position of the monopile. If the gripper frame fails beyond this point the monopile might tip over. This could lead to: a loss of the monopile, damage to the monopile and/or the vessel and a hazardous situation can occur possibly causing harm to crew members.
   As the monopile is standing in the soil, it acts as an inverted pendulum, i.e. the monopile will show unstable behavior if it is not kept in upright position by the gripper frame. Next, after a noise mitigation screen is installed, a vibro drill is connected to the crane hook instead of the ILT. This vibro drill is lifted on top of the monopile standing on the seabed to drive the monopile into the soil.

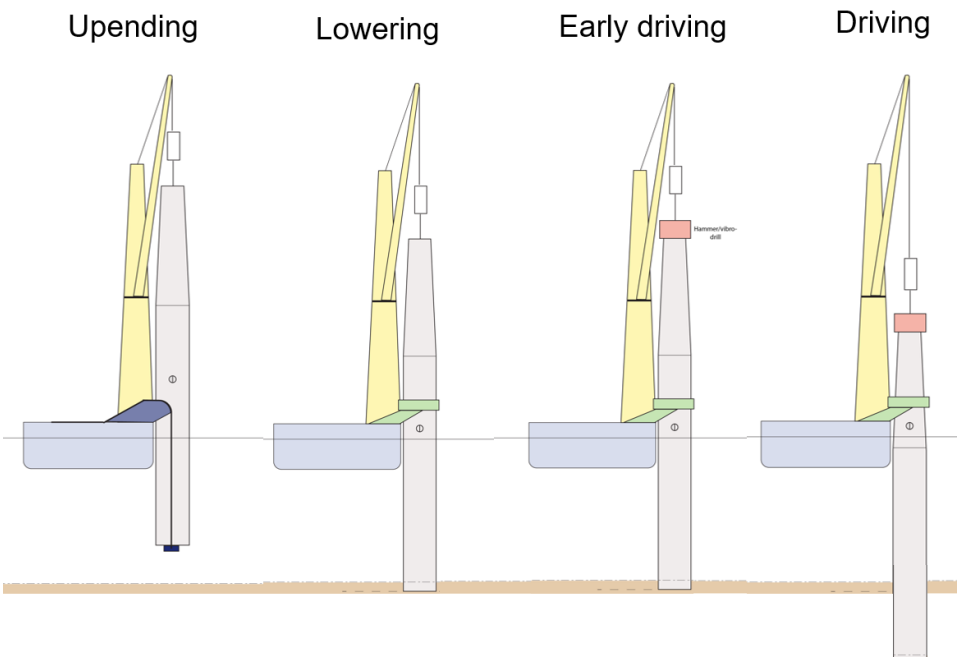

Figure 1.6: Monopile installation phases 2-5

5. **Driving the monopile and correcting for tilt**
   The monopile is driven into the soil to a penetration depth under which the monopile can maintain its upright position from monopile-soil interaction without the support of the gripper frame. During this pile driving, as the penetration depth increases, the monopile can start to induce mooring forces on the vessel. Next, the inclination is measured and corrected and the monopile gripper frame is disconnected from the monopile. Finally, the monopile is driven to its final penetration depth.
6. **Finish** After disconnecting the vibro drill, the installation is completed. The operation can be continued by installing a transition piece on top of the monopile depending on the installation strategy applied by the installation contractor.

Critical phase

The early pile driving phase (phase 4) of the monopile installation is considered the critical phase for the entire installation. For all other phases of installation, the procedure can be stopped when something goes wrong or when weather circumstances deteriorate to unacceptable limits. The monopile can be lifted back on the vessel, or it can be released when sufficient penetration depth is reached. This is not possible for the early driving phase.

1.3. Problem statement

HLCV Stella Synergy will soon be added to the fleet and it will be used to install monopiles. Jumbo Maritime is currently exploring what is the best monopile installation method for their vessel in terms of risk, workability and costs. Ideally, an installation is carried out with the use of DP as a station-keeping method for it shows a promising cut in installation time. However, since it is not yet decided what kind of DP-system will be equipped on HLCV Stella Synergy, it is not possible to investigate an installation with DP as a station-keeping method.

Installing monopiles from a floating vessel brings its challenges. During such installations, the vessel will inevitably move due to dynamic environmental forces. The severity of these motions and resulting forces determine the workability of the operation. The horizontal vessel motions must not exceed the design limits of the gripper frame. Also, the forces exerted by the gripper frame to hold the monopile upright can push the vessel from its set position. It is not yet known what the significance of this force is and if this affects the overall workability.

1.4. Research question

The objective of this research is to investigate what the limiting conditions are for the overall workability of a floating monopile installation and investigate measures to improve this workability. This results in the following main research question:

"What is the workability of the early pile driving phase of a monopile installation by using moorings as a station-keeping method and what is the influence of the gripper forces on this workability?"

In order to answer the main research question, the following sub-questions are composed:

- *"How does the vessel behave in irregular waves?"*
- *"How are the forces from the gripper frame computed during a monopile installation?"*
- *"What are the limiting criteria for a monopile installation?"*

1.5. Approach

In order to simulate the vessel motions, a linear model can be made in the frequency domain. Due to the presence of nonlinear phenomena in the system, like viscous drag forces and controller forces from the motion compensated gripper frame, the linear approach in the frequency domain is not sufficient. However, it is used in the determination of the motion equation for the time-domain simulations.

The approach to reach the objectives is visualized in Figure 1.7. An explanation of this approach is given in the Sections 1.5.1 through 1.5.3, which also highlight the outline of this thesis.

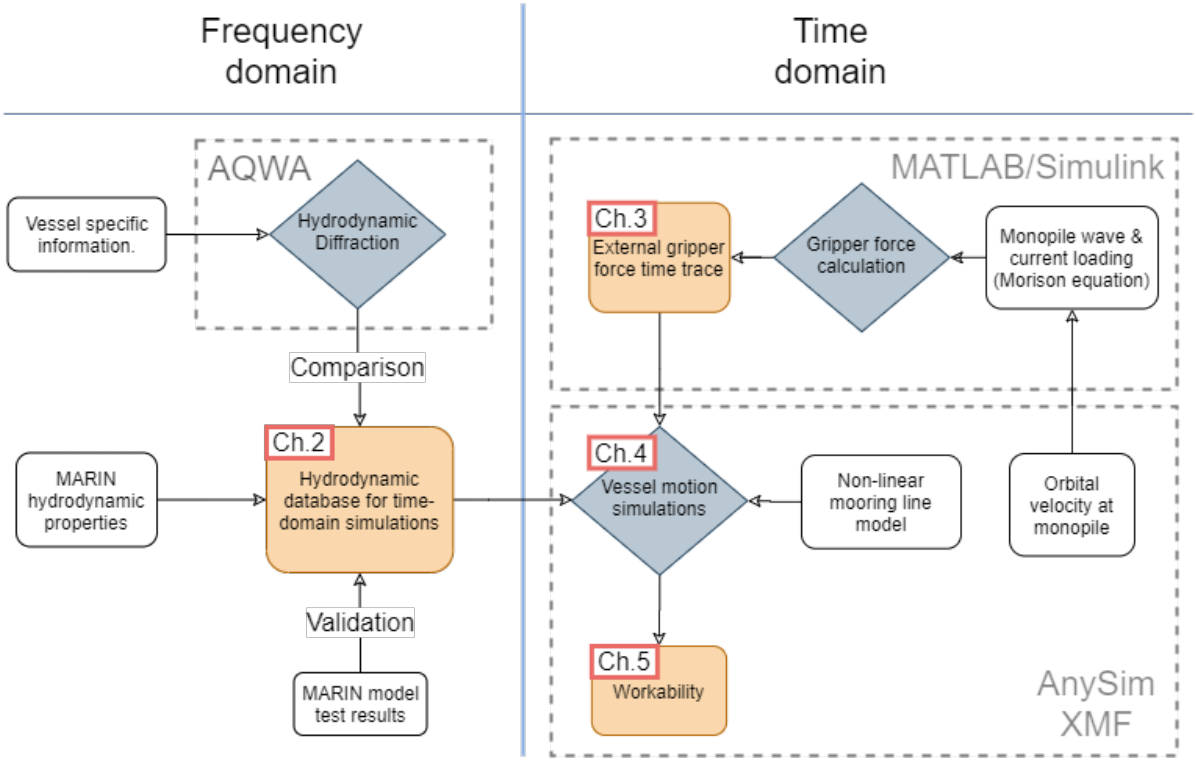

Figure 1.7: Flowchart of thesis approach

1.5.1. Create and validate a hydrodynamic database

Chapter 2 discusses how a hydrodynamic database is created which is used as input in time-domain simulation software AnySim XMF. This database contains Quadratic Transfer Function (QTF) values and added mass and damping values for 80 different wave frequencies and 72 different wave directions. The hydrodynamic database which is used in the simulations is provided by MARIN. A separate hydrodynamic database is created with diffraction software AQWA and the results are compared with the provided database. Also, a validation is performed with the results of a model basin seakeeping test performed by MARIN.

1.5.2. Gripper force time series

Chapter 3 discusses how time-series of external gripper forces are generated. First, the wave- and current loading on the monopile for a specific irregular sea state is derived. This is done by extracting the orbital velocity from a simulation in AnySim XMF and using the Morison equation to derive monopile loads from waves and current from this orbital velocity data. In a MATLAB/Simulink model, a 1 Degree of Freedom (DOF) model of the monopile is made and the motion compensated gripper controller applies control forces to maintain upright position of the pile. This gripper controller consists of a PID controller which is tuned so that the monopile is held in upright position in governing environmental conditions. Once the gripper controller is tuned, the MATLAB/Simulink model is able to generate a gripper force time series for every individual simulation. This gripper force time series is then applied as an external force to the vessel in the vessel motion simulations.

1.5.3. Workability calculation

The hydrodynamic database, provided by MARIN, is used as input for the in time-domain simulations in Anysim XMF. In these simulations the vessel motions are determined when subjected to irregular waves, current and external forces from the gripper frame. Also the mooring lines are simulated. The vessel is subjected to sea states that are common in the North sea, where a lot of wind turbines will be installed in the coming years. There are a number of limit criteria that must not be exceeded during the installation:

1. **Vessel motions**
   During the early driving phase the crane will lift the vibro drill on top of the monopile. During such a heavy lifting operation, the vessel roll and pitch motions must not become too large. This is due to the risk of swinging of the load due to this roll or pitch. A limit of 1 degree of roll and 1 degree of pitch is used.

2. **Mooring line tension**
   The tension of the mooring lines must remain below the maximum allowable tension. This maximum allowable tension is equal to the Minimum Breaking Load (MBL) divided by a Safety factor (S).

3. **Gripper reach**
   If the vessel moves 1 m in surge or sway direction, the gripper frame must 'reach' in the opposite direction for 1 m to compensate this vessel motion. However, the maximum allowable vessel motion in surge and/or sway is limited by the maximum reach of the gripper frame.

4. **Soil**
   During the early driving phase, the pile motions are limited by the plasticity of the soil. If the monopile exceeds the inclination limit, the soil will deform plastically and the monopile will not return to its vertical position. The inclination limit for a 10m diameter monopile is 0.5 degrees [Buitendijk, 2016]. This means that the monopile inclination angle cannot exceed 0.5 degrees during the entire installation phase.

5. **Monopile integrity**
   The gripper frame exerts restoring forces on the monopile to maintain a vertical position. These restoring forces must not exceed a limit to maintain monopile integrity and not cause damage to the monopile due to local pressure limits being exceeded.

1.6. Thesis scope

This research focuses on the floating installation of very large offshore wind turbine foundations (XL-monopiles). The focus is on the hydrodynamic behavior of the vessel with the monopile rather than operational issues or design issues.

The vessel has not been built yet. A model basin seakeeping test report executed by MARIN for HLCV Stella Synergy is used as reference for creating a hydrodynamic model of the vessel.

The early pile driving phase (phase 4) is considered critical in terms of risk. Therefore it is analyzed in this thesis. Pile handling and lowering are not incorporated in this research. In the critical phase, the monopile penetrates the seabed due to its self-weight. The connection between the monopile tip and the soil is modeled as a hinge, allowing rotations but no translations of the monopile tip. To this end, the lateral motion of the monopile tip is not addressed. As it is standing on the seabed, the monopile acts as an inverted pendulum and shows instable behavior if it is pushed out of vertical. The vibro drill, used to drive the monopile into the soil, is placed on top of the monopile and adds to this instable behavior. The monopile is assumed to be rigid.

The monopile and the vessel are subjected to environmental forces from wind, waves and current. The wave height at the location of the monopile can be reduced by shielding the incoming waves with the vessel. The reduction of wave height due to wave shielding effects is not addressed in this research. The workability is calculated for two different directions of incoming waves and current. This has been done by performing 3 hour time-domain simulations for each assessed sea state.

In this research, the location to install monopiles is the Central North Sea. A wave scatter diagram from this location is used for the workability analysis. This scatter diagram is based on wave data from an entire year. Also, the water depth, 40 m, is representative of locations in the Central North Sea where a lot of future wind turbines are planned to be installed.

2

Vessel motions

In this chapter it is depicted how a hydrodynamic database is created. The input needed for the simulation program AnySim XMF is provided by MARIN. However, a separate database is created with diffraction software AQWA and this is compared to the result of the provided database. Before the diffraction calculation is discussed, the coordinate system and heading conventions used throughout this thesis are depicted. Next, a validation is performed with the results from the model basin seakeeping tests performed by MARIN [MARIN and Jumbo Maritime, 2018]. All theory derivations made in this chapter are adopted from [Massie and Journée, 2001] unless mentioned otherwise.

2.1. Coordinate system

In Figure 2.1 and 2.1 the six degrees of freedom of a vessel are depicted. There are three translational and three rotational degrees of freedom which have its origin in the center of gravity.

DOF	Symbol	Description
Surge	x	Translation in x-direction
Sway	y	Translation in y-direction
Heave	z	Translation in z-direction
Roll	ϕ	Rotation around x-axis
Pitch	θ	Rotation around y-axis
Yaw	ψ	Rotation around z-axis

Table 2.1: Coordinate system description

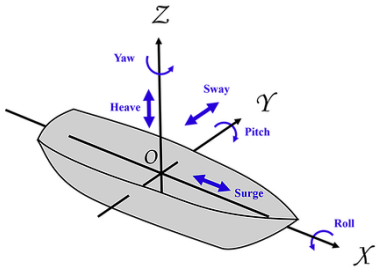

Figure 2.1: The six degrees of freedom of a vessel

The heading conventions used throughout this thesis are depicted in Figure 2.2.

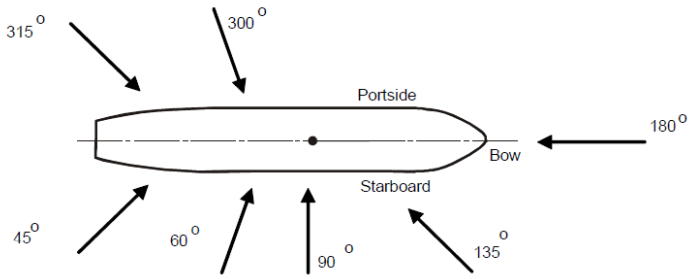

Figure 2.2: Heading conventions

2.2. AQWA Diffraction

This section describes the diffraction calculation in AQWA. A mesh is made of the vessel geometry, and the vessel specific information (see Appendix A.1) is used in the equation of motion.

2.2.1. Loading condition

The vessel specific information which is used in this research is based on a loading condition of the vessel with a high GM. This GM is the distance between the center of gravity and the metacenter of the vessel and it indicates the amount of hydrostatic restoring moment for roll motion. The loading condition with a high GM, which is used in this thesis, is considered as the most unfavorable loading condition in terms of vessel motions during an offshore installation.

2.2.2. Equation of motion

The total equation of motion of the vessel in frequency domain looks as follows:

$$\left(-\omega^2 \left(\mathbf{m} + \mathbf{a}(\omega)\right) + i\omega \left(\mathbf{b}(\omega) + \mathbf{B_{add}}\right) + C\right) \mathbf{X} = \mathbf{Fw} + \mathbf{F_D} \tag{2.1}$$

With:

- **m** = Vessel mass matrix
- **a**(ω) = added mass matrix (frequency dependent) due to radiation
- **b**(ω) = radiation damping matrix (frequency dependent)
- $\mathbf{B}_{add}$ = added viscous damping matrix
- **C** = Vessel stiffness matrix containing hydrostatic buoyancy characteristics
- **X** = Vessel position matrix
- $\mathbf{F}_W$ = Undisturbed wave forces
- $\mathbf{F}_D$ = Diffraction forces

The vessel specific data can be found in Appendix A.1.

2.2.3. Mass and hydrostatics

The vessel mass matrix looks as follows. As mentioned, there are 6 degrees of freedom.

$$\mathbf{m} = \begin{bmatrix} m & 0 & 0 & 0 & 0 & 0 \\ 0 & m & 0 & 0 & 0 & 0 \\ 0 & 0 & m & 0 & 0 & 0 \\ 0 & 0 & 0 & I_{xx} & 0 & 0 \\ 0 & 0 & 0 & 0 & I_{yy} & 0 \\ 0 & 0 & 0 & 0 & 0 & I_{zz} \end{bmatrix} \tag{2.2}$$

Where m is the vessel mass and I is the moment of inertia. The moments of inertia are calculated using: $I = mr^2$ where r is the radius of gyration of that particular degree of freedom. These radii of gyration are provided by Jumbo.

There are also hydrostatic buoyancy forces working on the vessel. These buoyancy forces act as a spring on the vessel and are therefore characterized as stiffness values in the vessel stiffness matrix C.

2.2.4. Radiation forces

When a body in water accelerates, it also accelerates water around the body generating radiated waves. To account for this radiation in the equation of motion an added mass matrix **a** is used. This added mass is frequency-dependent. The body is also damped by the water. This is represented in the radiation damping matrix **b** which is also frequency dependent. Both the added mass and damping values are calculated and provided by MARIN. Also a calculation is done in AQWA to support and validate the provided values. These calculations have been performed with potential theory described in [Massie and Journée, 2001]. Using this theory, water is assumed to be non-viscous, incompressible and irrotational.

2.2.5. Viscous damping

When the radiation forces are calculated, damping is introduced into the equation of motion. This radiation damping does not take into account viscous effects. Especially for roll damping, these viscous effects are significant and the calculated potential roll damping is generally relatively small. The viscous damping consists of: resistance due to bilge keels, eddy making and skin friction [Massie and Journée, 2001]. Multiple methods exist to estimate the roll damping, however it is also possible to determine the roll damping from experimental model scale tests. In this thesis, the roll damping is calculated based on the results of experimental tests [MARIN and Jumbo Maritime, 2018]. The calculated roll damping is added to the model to obtain similar roll motions compared to the results from the model tests.

2.2.6. Incoming wave and diffraction forces

Due to the presence of a body in water, a wave field is disturbed and thus diffracted. This diffraction causes a force on the body. The total forces a wave transfers to a body in water consists of the undisturbed wave forces and the diffraction forces. The flow potential from an undisturbed wave in deep water is:

$$\Phi_0 = -\frac{\zeta_a g}{\omega} e^{kz} \sin(\omega t - kx\cos(\mu) - ky\sin(\mu)) \tag{2.3}$$

Where ζ_a is the wave amplitude, k is the wave number and μ is the incoming wave direction. From here the pressure is calculated according to:

$$p_{\Phi_0+\Phi_7} = -\rho \frac{\partial\,(\Phi_0 + \Phi_7)}{\partial t} \tag{2.4}$$

Where the undisturbed wave potential Φ_0 and diffraction potential Φ_7 are calculated using the panel method in diffraction software. This panel method is explained in [Massie and Journée, 2001]. The total undisturbed wave forces and diffraction forces can then be calculated by integrating the pressure over the entire surface:

$$F_D + F_W = \iint_S \left(p_{\Phi_0+\Phi_7} f\right) dS \tag{2.5}$$

2.3. Validation

In this section, the hydrodynamic database is validated against the results of the model scale tests. This is done by highlighting the results of the AQWA calculation compared to the results from the model tests. The hydrodynamic database, which is later used in AnySim XMF, is provided by MARIN and it is generated with diffraction program DIFFRAC. The AQWA calculation serves as a comparison with the DIFFRAC calculation.

The full equation of motion (Equation 2.1) is now known and it can be solved. A frequency-dependent Response Amplitude Operator (RAO) is derived, which is a transfer function between the wave height and the response in the corresponding DOF. This response is dependent on the frequency of the incoming wave and the direction of the incoming wave. The wave directions are depicted in the heading conventions in Figure 2.2.

2.3.1. RAOs

During the MARIN seakeeping measurements a scale model of the vessel is used. During the measurements a wave spectrum S_ζ with a significant wave height Hs and peak period Tp is used. [MARIN and Jumbo Maritime, 2018] states that the measured motion spectrum of the vessel S_u is then used to calculate the RAO by the following:

$$RAO = \sqrt{\frac{S_u}{S_\zeta}} \tag{2.6}$$

In the seakeeping measurements, the heave, pitch and roll RAOs are measured. Figures 2.3 - 2.5 show the calculated RAOs of heave, pitch and roll from the AQWA model and these are compared to the measurements from the model tests. It can be seen that the model test results are depicted with a particular sea condition (combination of Hs and Tp). During the measurements, the vessel scale model was subjected to (irregular) waves, derived from these particular sea conditions.

2.3.2. Heave

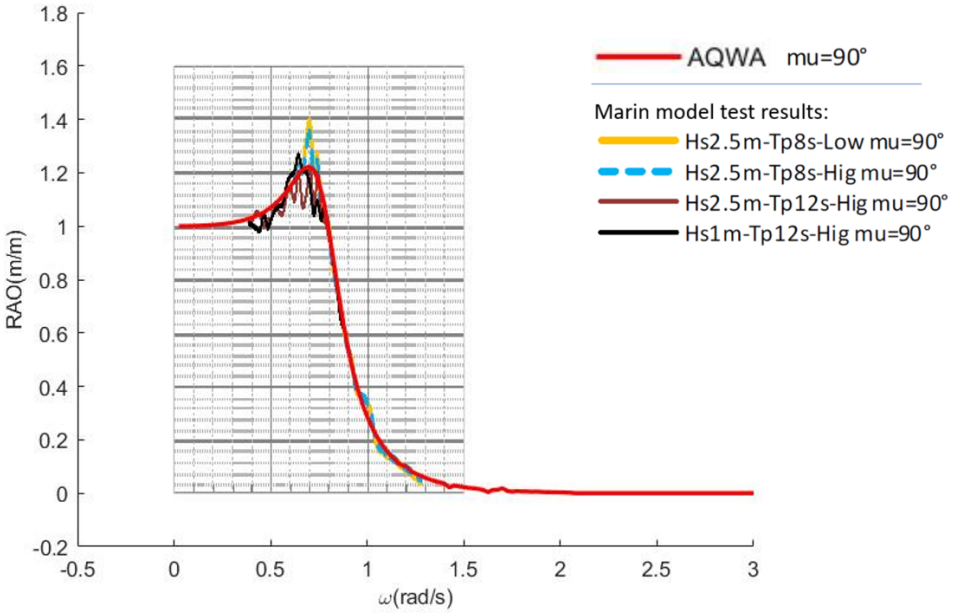

Figure 2.3: Heave RAO compared to MARIN results per frequency for an incoming wave direction of μ = 90°

The largest heave responses are observed for beam waves ($\mu = 90°$), which is why the displayed AQWA results are taken from the same incoming wave direction. In Figure 2.3, four different results from the model tests (yellow, blue, brown and black lines) are visualized together with the results from AQWA (red line). The result which is depicted with 'Low' (in Figure 2.3 that is the yellow line) is for a loading condition with a low GM value. In this thesis, only the high GM results are considered.

It can be seen in Figure 2.3 that the calculated RAOs from AQWA are very similar to the measured RAOs from the model tests. However, some small differences are present. As mentioned, the measurements are performed during irregular sea conditions. Due to the irregularity in the sea conditions used in the measurements, the results can show small deviations compared to the results of the AQWA calculation. Although the results have small differences, the AQWA calculation is considered a representative average value of the heave RAO.

2.3.3. Pitch

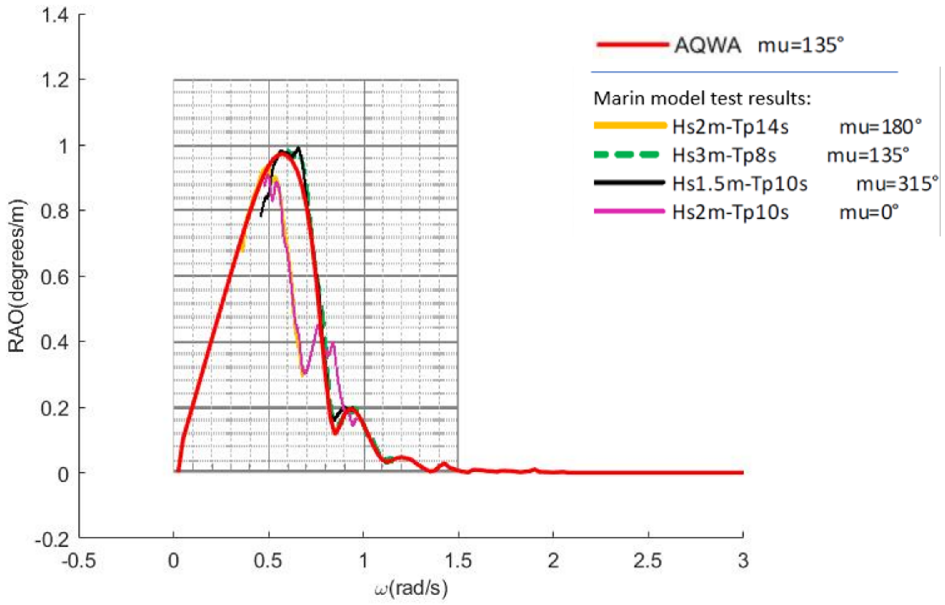

Figure 2.4: Roll RAO compared to MARIN results per frequency for an incoming wave direction of μ = 135°

The largest pitch responses are observed for $\mu = 135°$. The calculated Pitch RAOs in AQWA are also very similar to the results from the model tests. In Figure 2.4 the MARIN model test results are visualized for different incoming wave directions μ. The green dotted line is in the same direction as the AQWA RAOs. It can be seen that this green dotted line and the AQWA results (red line) are almost exactly the same. Which is why it is concluded that the calculated Pitch RAO is a representative result compared to the model test results.

2.3.4. Roll

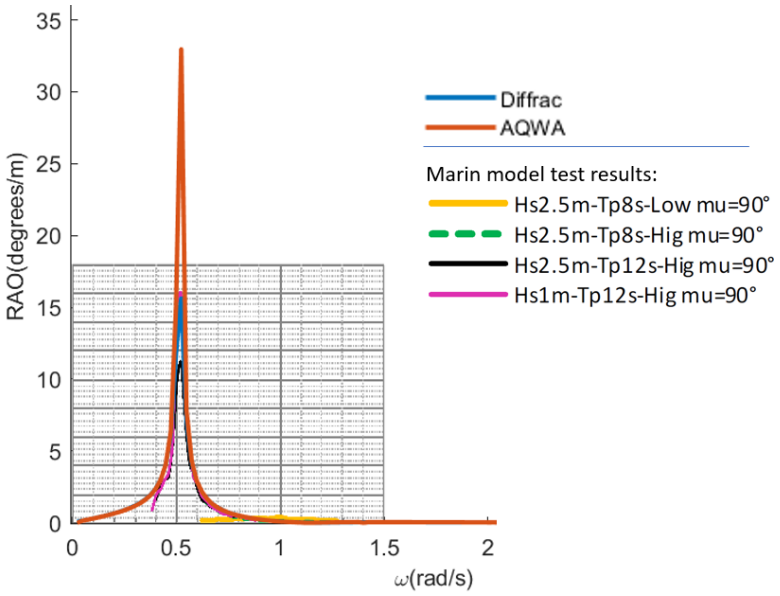

Figure 2.5: Roll RAO compared to MARIN results per frequency for an incoming wave direction of μ = 90°

It can be seen in Figure 2.5 that the peak of the RAO calculated in AQWA is much higher than the measured RAO from the model tests. The high peak at the roll natural frequency (ω = 0.52 rad/s) indicates there is not much damping in the calculations from AQWA. As explained in Section 2.2.5, this is because no viscous damping is incorporated in the AQWA calculation. This problem is solved by calculating the viscous damping and adding this to the model to obtain similar roll response compared to the model test results. In the hydrodynamic database (generated with diffraction program DIFFRAC), which is later used in AnySim XMF, this viscous damping is added in the calculation and the result is also visualized in Figure 2.5. It can be seen that the DIFFRAC results, where viscous damping is added, are similar to the model test results.

3

Gripper force calculation

In this chapter, the method to derive the horizontal gripper forces is discussed. This consists of three parts.

1. First, a 1-DOF model of the monopile is made in MATLAB/Simulink and the motion compensated gripper controller applies control forces to maintain upright position of the pile.
2. The gripper frame controller is a PID controller which is tuned so that the monopile is held in upright position when subjected to governing environmental conditions.
3. Finally, a gripper force time series can be computed for every individual simulation.

3.1. Monopile model

This section describes the monopile model in MATLAB/Simulink. This model includes a mathematical representation of the monopile, the vibro drill and the trapped water inside the monopile. The model describes the behavior of the monopile under the influence of environmental loads, self-weight and control forces applied by the gripper frame. This is captured in a one DOF system which is visualized in Figure 3.1.

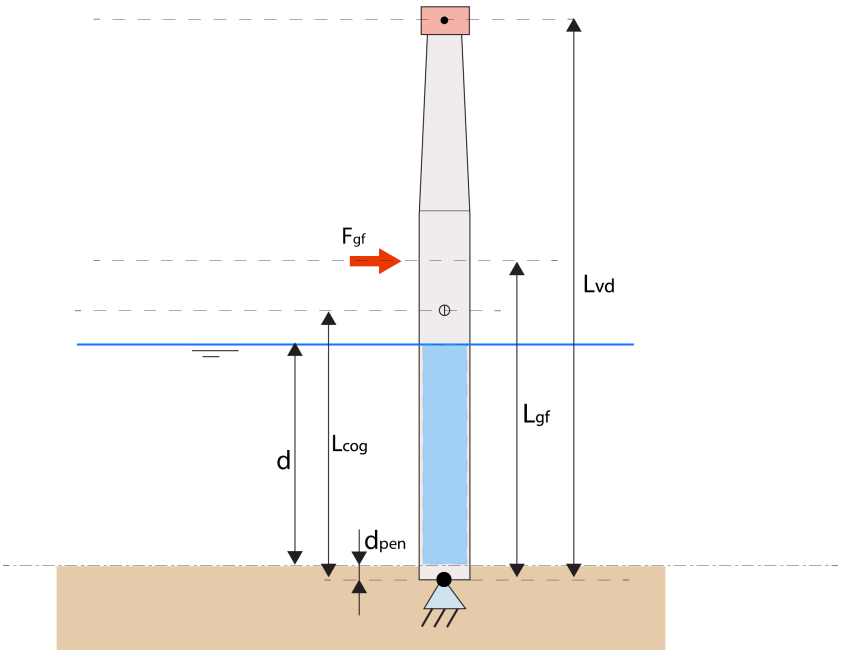

Figure 3.1: Simplified monopile model

The equation of motion of an inverted pendulum around a pivot point is given by:

$$I * \ddot{\alpha} + b * \dot{\alpha} + k_{to} * \alpha = M \tag{3.1}$$

Where:

- α = the rotation angle of the monopile around the fixed pivot point.
- I = the total moment of inertia of the system.
- b = the hydrodynamic rotational damping which is neglected in this simplified model.
- k_{to} = the rotational tipping over stiffness.
- M = the moment around the pivot point from environmental forces and forces from the gripper frame.

Above mentioned variables for the equation of motion are highlighted in the rest of this section:

The **moment of inertia** of the monopile I_{mp}, the trapped water inside the monopile I_{tw} and the vibro drill I_{vd} together form the total moment of inertia I:

$$I_{mp} = \frac{1}{3} * m_{mp} * L_{mp}^2, \qquad I_{tw} = \frac{1}{3} * m_{tw} * d^2, \qquad I_{vd} = m_{vd} * L_{vd}^2 \tag{3.2}$$

$$I = I_{mp} + I_{tw} + I_{vd} \tag{3.3}$$

Now, the **rotational stiffness** k_{to} is discussed. In this model, the rotational stiffness due to monopile-soil interaction is neglected. Due to the tipping over tendency of the inverted pendulum this stiffness is negative.

$$M_{to} = k_{to} * \alpha \tag{3.4}$$

Where M_{to} is the **tipping over moment** and k_{to} is the tipping over rotational stiffness. In Equation 3.4, the goniometric relation is approximated by a linear relation due to small angles: $sin(\alpha) \approx \alpha$. The error of this approximation is 1% for an angle of 14 deg. Since a large angle of 14 deg will never be reached in the simulations, the error is assumed to be acceptable.

An offset of the center of gravity from default position (vertical position) results in a moment around the pivot point. The monopile and the vibro drill both contribute to this moment.

$$M_{to} = \alpha * -(L_{cg} * m_{mp} * g + L_{vd} * m_{vd} * g) \tag{3.5}$$

Now, the following equation follows from Equation 3.4 and 3.5:

$$k_{to} = -(L_{cg} * m_{mp} * g + L_{vd} * m_{vd} * g) \tag{3.6}$$

The values used in the simulation are summarized in Table 3.1.

Monopile properties	**I** (kg*m^2)	**b** (Nm*s/rad)	$\mathbf{k}_{to}$ (Nm/rad)
m_{mp} = 2100 tonnes			
m_{vd} = 1000 tonnes			
d = 40m			
d_{pen} = 4m	1.47e+10	0	-1.97e+09

Table 3.1: Monopile model specific information

Next, the **total external moment** M is discussed. This external moment consists of restoring forces from the gripper frame and environmental forces from waves and current. Wind forces are neglected for this simplified model.

$$M = M_{cu} + M_w + M_{GF} \tag{3.7}$$

The moment from the gripper frame M_{GF} is calculated as follows: $M_{GF} = F_{GF} * L_{GF}$. The gripper frame control forces F_{GF} are discussed in Section 3.2.

The moment from current M_{cu} and waves M_w are determined in two steps. The first step is to generate an orbital velocity time series at the exact location of the monopile. This location is highlighted in red in Figure 3.2. This orbital velocity time series is extracted from a simulation in AnySim XMF where an imaginary wave probe, placed at the location of the monopile, measures the orbital velocity. The second step is to use this orbital velocity time series and apply the Morison equation [Massie and Journée, 2001] to determine the total moment on the monopile due to wave- and current forces.

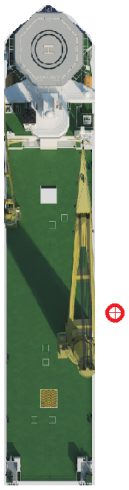

Figure 3.2: Wave probe location compared to HLCV Stella Synergy (top view)

3.2. Gripper frame controller

The gripper frame has to be able to compensate the vessel motions and maintain vertical position for the monopile when the vessel is exposed to governing environmental conditions. These governing environmental conditions (depicted in Table 3.2) are considered the roughest conditions under which the gripper frame must be able to perform its task [Jumbo Maritime, 2019]. In the MATLAB/Simulink model, a gripper frame controller is incorporated. This gripper frame controller must first be tuned in order to function under these governing conditions.

Description	Symbol	Value	Unit
Significant wave height	H_s	2.0	m
Peak period	T_p	8.0	sec
Current velocity	$v_{current}$	1.5	kn

Table 3.2: Governing environmental conditions

Controller tuning

Now, the governing environmental conditions from Table 3.2 are used to extract an orbital velocity time series. The current loading M_{cu} and wave loading M_w time series are derived from this orbital velocity.

The tuning of the gripper frame controller is based on two boundary conditions. These boundary conditions are directly related to limiting criteria (number 4 and 5) which are mentioned in Section 1.5.3 and repeated here:

1. The monopile inclination angle has to remain within the limit of 0.5 degrees.
2. The maximum applied gripper force must not exceed a limit to maintain monopile integrity. This limit is listed in Appendix A.3.

Based on the governing environmental conditions, the Proportional (P), Integral (I) and Derivative (D) gains of the PID-controller are chosen such that the monopile motions and gripper forces remain within the boundary conditions. Once the gripper frame controller is tuned, the monopile model is able to produce a gripper force time series.

3.3. Gripper force time series

In Chapter 4 it is explained which environmental conditions (combinations of Hs, Tp and incoming wave direction μ) are considered in the vessel motion simulations. For each of these simulations a separate gripper force time series is applied. So for each simulation, the following is done:

- The orbital velocity time series is extracted from a simulation in AnySim XMF with a wave probe at the monopile location. This orbital velocity time series is converted to a wave- and current loading time series.
- The MATLAB/Simulink model simulates the monopile motions due to this wave- and current loading, and calculates the control forces applied by the gripper frame. This results in a gripper force time series.
- This gripper force time series is applied to HLCV Stella Synergy during the simulations. These simulations are described in Chapter 4.

4

Simulation setup

Now the hydrodynamic database and the external forces from the gripper frame are known. This chapter discusses how the environmental forces from waves, current and wind and the restoring forces from the mooring lines are transferred to the vessel in the time-domain simulation program AnySim XMF.

4.1. Environmental loads

This section describes how AnySim XMF calculates the environmental loads from waves, current and wind in the simulations.

4.1.1. Waves

The ocean surface can be described by the sum of multiple waves with each a different height, period, shape and direction. First a measured wave record is translated into a series of regular waves. This is then translated into a wave spectrum that describes the energy density as a function of the wave frequency. The JONSWAP spectrum is a widely used spectrum to generate waves representative of the North Sea, where a lot of future wind turbine installations are planned. The shape of the JONSWAP spectrum for a given significant wave height H_S and peak period T_P is given by:

$$S_{JONSWAP}(\omega) = \frac{320 H_{1/3}^2}{T_p^4} \omega^{-5} \exp\left(\frac{-1950}{T_p^4} \omega^{-4}\right) \gamma^A \tag{4.1}$$

with:

- $\gamma = 3.3$ (peakedness factor)
- $A = \exp\left(-\left(\frac{\frac{\omega}{\omega_p}-1}{\sigma\sqrt{2}}\right)^2\right)$
- $\omega_p = \frac{2\pi}{T_p}$
- $\sigma =$ a step function of ω: if $\omega < \omega_p$ then $\sigma = 0.07$, else: $\sigma = 0.09$

With inverse Fast Fourier Transform, the wave spectrum can be translated into a series of sinusoidal regular waves. By superposition of these series of regular waves, a wave elevation plot can be constructed in the time-domain according to Figure 4.1. The wave kinematics (water particle velocity and acceleration) corresponding to this superposed series of waves is dependent on wave height, water depth and other wave parameters. These wave kinematics can be calculated according to [Massie and Journée, 2001].

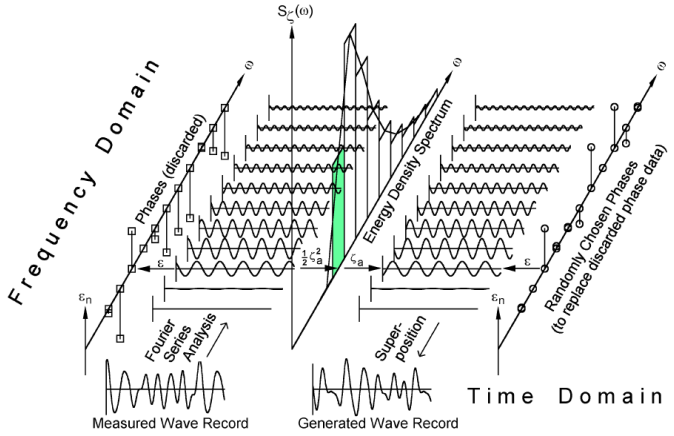

Figure 4.1: Wave record analysis and regeneration [9]

4.1.2. Current

The current force contributes to the vessel surge, sway and yaw motion. The current forces are calculated for a given current velocity U by using:

$$F_x = \frac{C_x}{\frac{1}{2}\rho U^2 \cdot T \cdot B}, \qquad F_y = \frac{C_y}{\frac{1}{2}\rho U^2 \cdot T \cdot L_{pp}}, \qquad M_z = \frac{C_\psi}{\frac{1}{2}\rho U^2 \cdot T \cdot L_{pp}^2} \tag{4.2}$$

with T, B and L_{pp} representing the vessel draught, breadth and length at the waterline respectively. The current force coefficients for all incoming wave directions are provided and are found in Appendix C.1.

4.1.3. Wind

The wind loads are calculated in a similar fashion as the current loads:

$$C_x = \frac{F_x}{\frac{1}{2}\rho U_{10}^2 \cdot A_F}, \qquad C_y = \frac{F_y}{\frac{1}{2}\rho U_{10}^2 \cdot A_S}, \qquad C_\psi = \frac{M_z}{\frac{1}{2}\rho U^2 \cdot A_S \cdot L_{pp}} \tag{4.3}$$

A_F and A_S are the frontal and sideways area of the vessel above the waterline and U_{10} is the reference wind velocity at $10m$ above water level. The wind force coefficients for surge, sway and yaw are provided (see Appendix C.2).

4.2. Mooring arrangement

During the monopile installation, HLCV Stella Synergy is moored to the seabed with 8 mooring lines. The direction in which these lines are deployed is visualized in Figure 4.2.

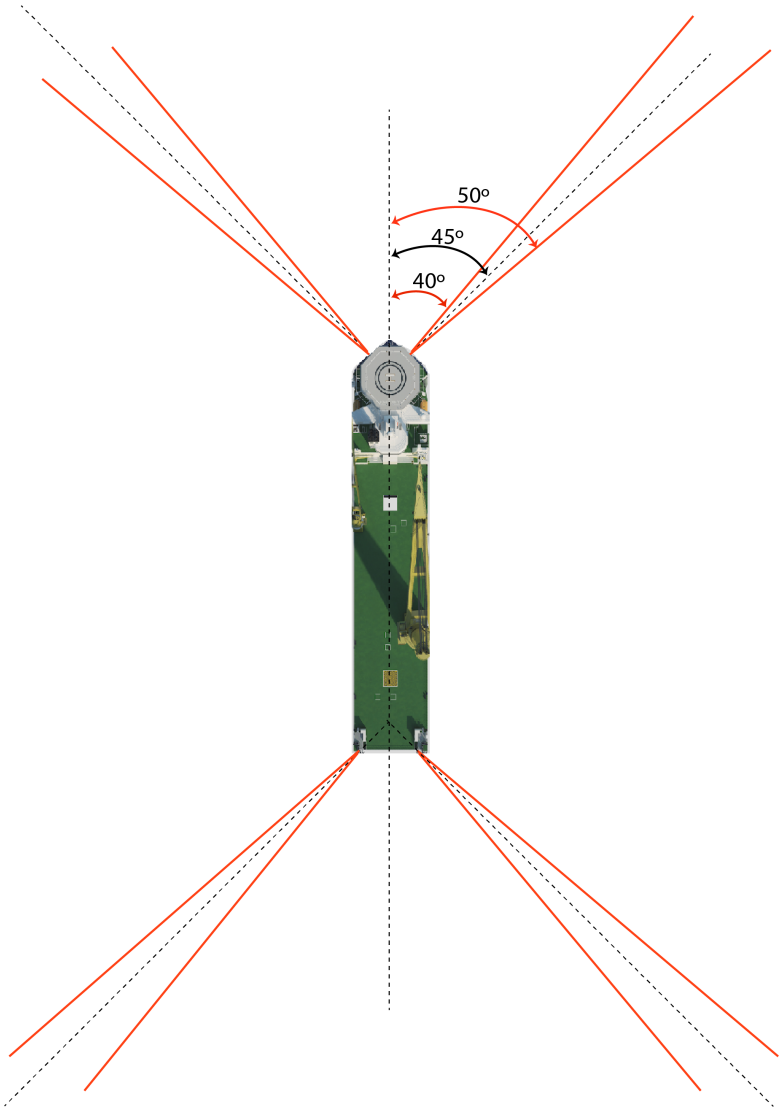

Figure 4.2: Arrangement of mooring lines

The mooring lines consist of two segments of different materials. The mooring line properties and applied pre-tension can be found in Appendix A.4.

4.3. Simulations

In Appendix B a scatter diagram of the North sea is visualized. It shows the probability of occurrence of every possible wave condition (Tp and Hs). All of these wave conditions are tested in the simulations: Hs = 0.25 m to 5.5 m and Tp = 3 s to 14 s. A constant current velocity v_{cu} of 1.5 kn is assumed during all simulations. The wind velocity v_{wind} varies with Hs based on the Beaufort scale [Massie and Journée, 2001] i.e. for a larger Hs a larger v_{wind} is chosen according to the Beaufort scale. The duration of one simulation is set to 3 hours. This is done to achieve stationary irregular wave conditions [DNV-RP-C205, 1993].

The incoming direction of the waves, wind and current are assumed co-linear and two different incoming directions are simulated. The incoming direction of the waves, current and wind are simulated for beam waves (μ=90 degrees) and for head waves (μ=180 degrees). In reality, the waves do not come from a single direction but there is some directional spreading. It is possible to apply this directional spreading in AnySim XMF, but this adds computational effort to the simulations. To account for this directional spreading, the incoming direction of the waves, current and wind is shifted 15 degrees [Jumbo Maritime, 2019]. This results in the directions of environmental forces depicted in Figures 4.4 and 4.3.

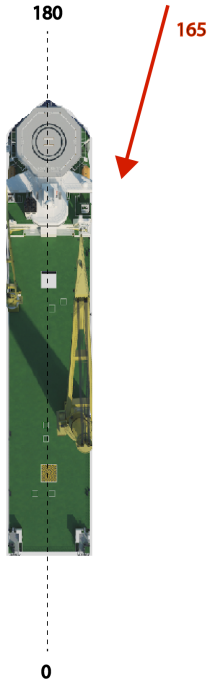

Figure 4.3: Direction environmental forces load case 2

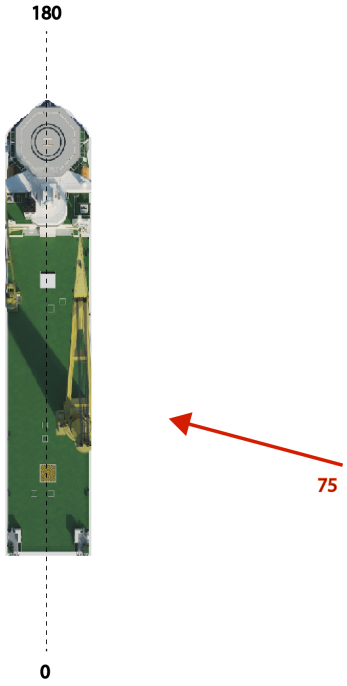

Figure 4.4: Direction environmental forces load case 1

5

Results

Before the results of the simulations are discussed, a summary is given of the assumptions and simplifications that are made in this research. This summary underlines the influence of these assumptions and simplifications on the results. In Chapter 6, the validity of these assumptions and simplifications are discussed. The workability is calculated for four limiting criteria, which are discussed before the results are presented.

5.1. Assumptions and simplifications

In this research, a number of assumptions and simplifications are made. These assumptions and simplifications apply to the components which are highlighted in Figure 5.1. In this Figure, the early driving phase of an XL-Monopile installation is visualized.

Figure 5.1: Overview of simplifications and assumptions

The components highlighted with numbers 1 until 5 in Figure 5.1 are now discussed:

1. Incoming direction of wind, waves and current

The environmental forces from wind, waves and current are assumed to come from one single direction. In reality, the direction of these environmental forces varies in time. In this research, a worst case scenario is analyzed by assuming a co-linear incoming direction for the wave, wind and current loading. This is done for two different incoming directions.

2. Motion compensated gripper frame

- The gripper frames that are currently used in the industry mostly consist of hydraulic cylinders that provide the reaction forces on the monopile. In reality these hydraulic cylinders have a dynamic pressure build-up before a certain target force is applied. In this research, this dynamic pressure build-up is not incorporated and the forces from the gripper frame are derived from a static analysis. The result is that the target force from the gripper frame controller is achieved instantaneously.

- The behavior of the gripper frame is modeled by performing an iteration. First, a time series of the environmental loading on the monopile is derived for a three hour simulation. Next, the gripper forces are determined by the gripper frame controller and a time series of these forces is created. This time series is then applied to the vessel during the vessel motion simulations.

3. Vessel loading condition

- The loading condition which is chosen to be analyzed is based on a high GM value. This high GM resembles the loading condition which is assumed most unfavorable in terms of roll motion. One can compare this High GM loading condition with the moment when the ballast tanks are completely filled. This is done to shift the total CoG of the vessel downwards. Because then, when a load is lifted by the crane (and the CoG of the load is assumed to be at the crane tip), the total CoG shifts upwards again resulting in a lower, and more favorable, GM value. This research focuses on the worst case scenario, which is why a high GM loading condition is analyzed.

- The viscous damping which is added to the hydrodynamic database was derived from experimental tests [MARIN and Jumbo Maritime, 2018]. These experimental tests are done with a scale model of the vessel in a water basin. It is possible that the actual viscous damping (once the vessel is built) differs from the viscous damping which is derived from the experimental tests.

4. Mooring lines

The mooring lines provide the station-keeping during the installation. These mooring lines can consist of different sections from a wide range of materials. Also, one can influence the station-keeping performance by changing the number of deployed mooring lines and by changing the direction in which the lines are deployed. In this research, only one mooring arrangement (discussed in Section 4.2) is tested.

5. Monopile

- The monopile is assumed rigid when determining the monopile motions.

- At the monopile tip in the soil, a hinge is assumed i.e. the lateral motions of the monopile tip are not addressed.

- Due to the presence of the vessel, the incoming waves are disturbed due to diffraction and radiation effects, resulting in a wave field with reduced wave height in the wake of the vessel with respect to the incoming wave direction. This effect is called wave shielding and it is not taken into account in this research. The environmental loading from waves on the monopile is based on the undisturbed incoming wave loading without diffraction and radiation effects from the vessel.

5.2. Workability limit criteria

In the coming Sections, the results are presented. Table 5.1, gives an overview of the load cases that are used in this research. Furthermore, this Section describes how the results are presented.

Load case	Incoming direction [°]	Forces from gripper frame
Load case 1	165	Included
Load case 2	75	Included
Load case 3	165	Not included
Load case 4	75	Not included

Table 5.1: Load cases

For all load cases, workability Figures are presented for the following limiting criteria:

1. Roll
2. Pitch
3. Tension in the mooring lines
4. Maximum horizontal distance from setpoint
5. Total workability combining all above mentioned limits

In the Figures, it is highlighted for all sea conditions (a sea condition is a combination of Hs and Tp) whether the limit in question is exceeded and the installation is thus not workable. The probability of occurrence from the scatter diagram (Appendix B) is projected over all sea conditions that are found to be workable. A sea condition is found to be workable if the limit in question is not exceeded during the entire simulation.

Next to the workability graphs, the calculated workability is mentioned. The workability is calculated by taking the sum of the probability of occurrence of all sea conditions that are found workable.

5.3. Load case 1: Workability with gripper forces - 165 degrees

In Figures: 5.2 through 5.6 the calculated workability for Load case 1 is visualized.

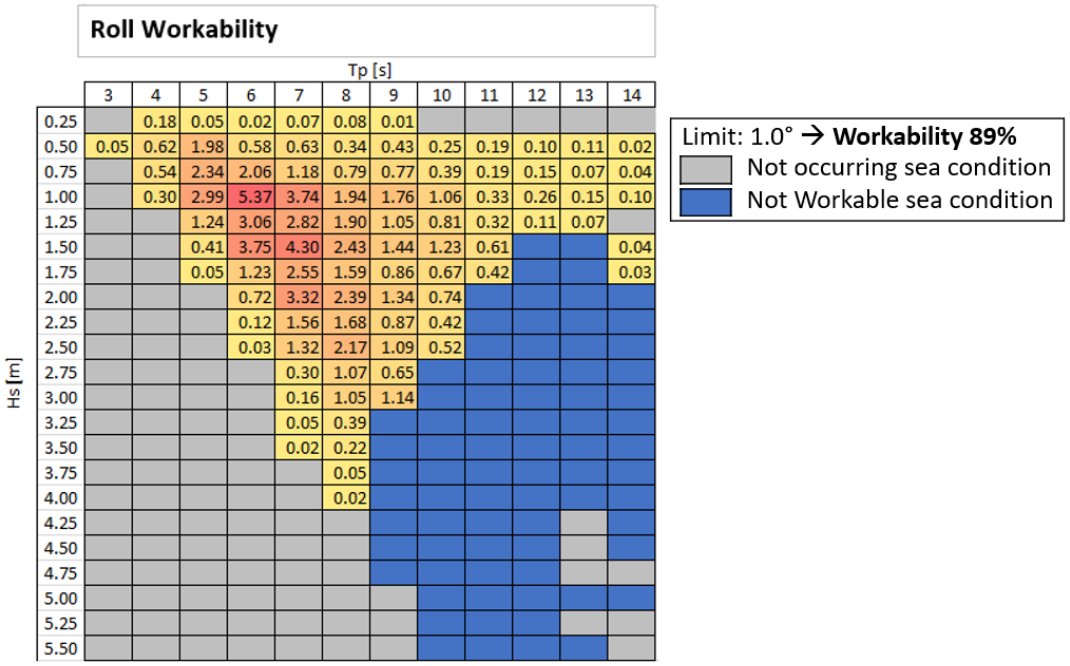

Figure 5.2: Head waves: Workability: Roll

Figure 5.2 shows that the roll motions, under the incoming sea direction of 165 degrees, are relatively mild. This is because the roll motions stay within the 1.0 degree limit for relatively rough conditions (for instance Hs = 2.50, Tp = 10s). The roll motions in sea conditions with a relatively high probability of occurrence (between Hs = 0.0 - 2.5m and Tp = 3.0 - 8.0s) all remain below the limit. This results in a workability of 89%.

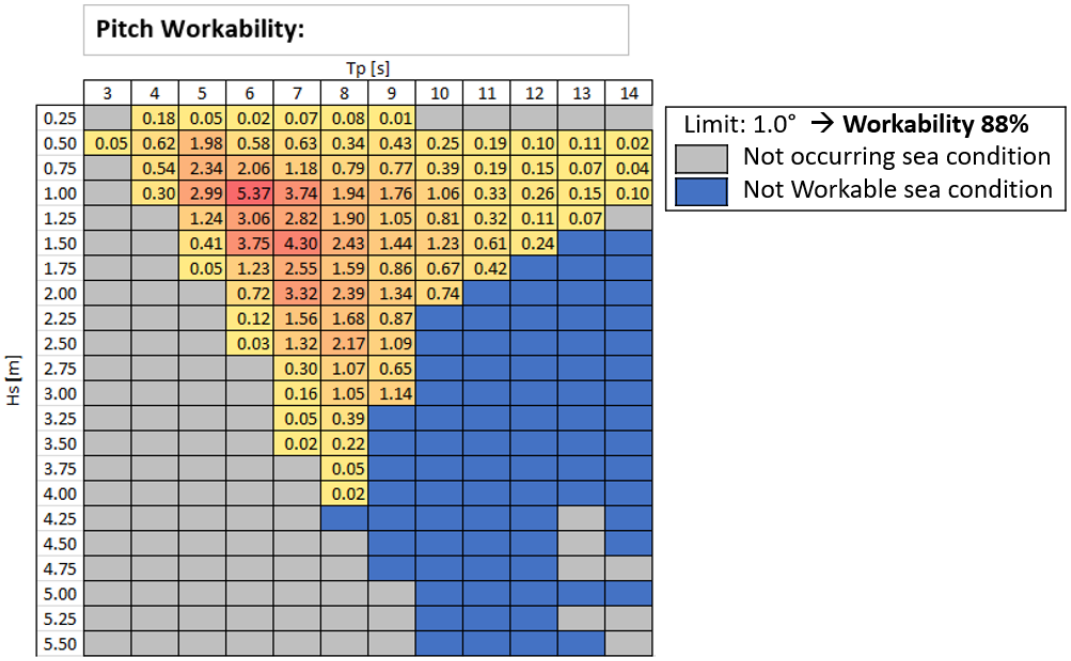

Hs [m] \ Tp [s]	3	4	5	6	7	8	9	10	11	12	13	14
0.25		0.18	0.05	0.02	0.07	0.08	0.01					
0.50	0.05	0.62	1.98	0.58	0.63	0.34	0.43	0.25	0.19	0.10	0.11	0.02
0.75		0.54	2.34	2.06	1.18	0.79	0.77	0.39	0.19	0.15	0.07	0.04
1.00		0.30	2.99	5.37	3.74	1.94	1.76	1.06	0.33	0.26	0.15	0.10
1.25			1.24	3.06	2.82	1.90	1.05	0.81	0.32	0.11	0.07	
1.50			0.41	3.75	4.30	2.43	1.44	1.23	0.61	0.24		
1.75			0.05	1.23	2.55	1.59	0.86	0.67	0.42			
2.00				0.72	3.32	2.39	1.34	0.74				
2.25				0.12	1.56	1.68	0.87					
2.50				0.03	1.32	2.17	1.09					
2.75					0.30	1.07	0.65					
3.00					0.16	1.05	1.14					
3.25					0.05	0.39						
3.50					0.02	0.22						
3.75						0.05						
4.00						0.02						
4.25												
4.50												
4.75												
5.00												
5.25												
5.50												

Figure 5.3: Head waves: Workability pitch

A similar result is found for the pitch motions in head waves compared to the roll motions. The pitch motions exceed the limit only in relatively rough conditions.

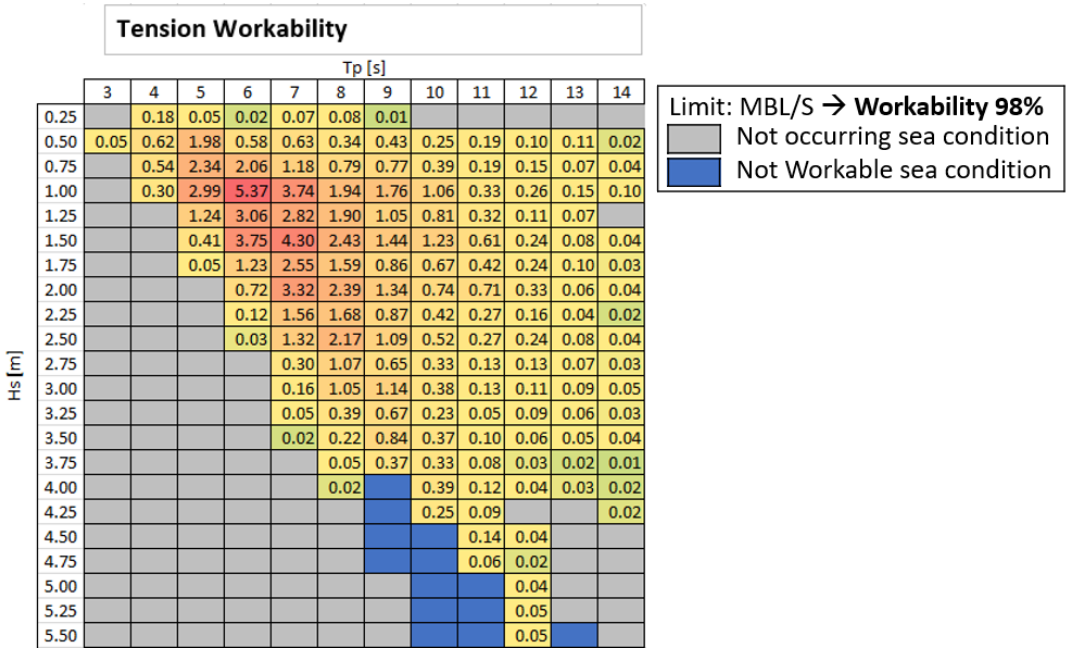

Hs [m] \ Tp [s]	3	4	5	6	7	8	9	10	11	12	13	14
0.25		0.18	0.05	0.02	0.07	0.08	0.01					
0.50	0.05	0.62	1.98	0.58	0.63	0.34	0.43	0.25	0.19	0.10	0.11	0.02
0.75		0.54	2.34	2.06	1.18	0.79	0.77	0.39	0.19	0.15	0.07	0.04
1.00		0.30	2.99	5.37	3.74	1.94	1.76	1.06	0.33	0.26	0.15	0.10
1.25			1.24	3.06	2.82	1.90	1.05	0.81	0.32	0.11	0.07	
1.50			0.41	3.75	4.30	2.43	1.44	1.23	0.61	0.24	0.08	0.04
1.75			0.05	1.23	2.55	1.59	0.86	0.67	0.42	0.24	0.10	0.03
2.00				0.72	3.32	2.39	1.34	0.74	0.71	0.33	0.06	0.04
2.25				0.12	1.56	1.68	0.87	0.42	0.27	0.16	0.04	0.02
2.50				0.03	1.32	2.17	1.09	0.52	0.27	0.24	0.08	0.04
2.75					0.30	1.07	0.65	0.33	0.13	0.13	0.07	0.03
3.00					0.16	1.05	1.14	0.38	0.13	0.11	0.09	0.05
3.25					0.05	0.39	0.67	0.23	0.05	0.09	0.06	0.03
3.50					0.02	0.22	0.84	0.37	0.10	0.06	0.05	0.04
3.75						0.05	0.37	0.33	0.08	0.03	0.02	0.01
4.00						0.02		0.39	0.12	0.04	0.03	0.02
4.25								0.25	0.09			0.02
4.50									0.14	0.04		
4.75									0.06	0.02		
5.00										0.04		
5.25										0.05		
5.50										0.05		

Figure 5.4: Head waves: Workability Mooring line tension

The mooring line tension workability is visualized. There are 8 mooring lines, and if the tension in at least one of these lines exceeds the limit, then the installation is not workable. This is incorporated in the workability, which is visualized in Figure 5.4. It can be seen that the tension in (at least one of) the mooring lines does not exceed the limit for nearly all simulated sea condition, resulting in a workability of 98%.

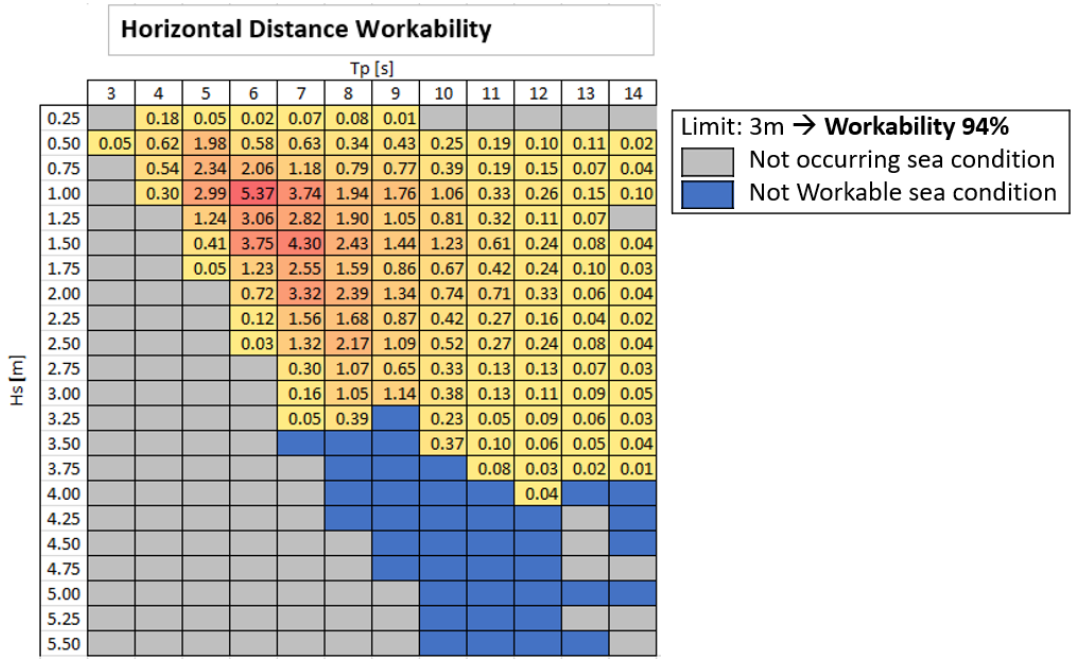

Hs [m] \ Tp [s]	3	4	5	6	7	8	9	10	11	12	13	14
0.25		0.18	0.05	0.02	0.07	0.08	0.01					
0.50	0.05	0.62	1.98	0.58	0.63	0.34	0.43	0.25	0.19	0.10	0.11	0.02
0.75		0.54	2.34	2.06	1.18	0.79	0.77	0.39	0.19	0.15	0.07	0.04
1.00		0.30	2.99	5.37	3.74	1.94	1.76	1.06	0.33	0.26	0.15	0.10
1.25			1.24	3.06	2.82	1.90	1.05	0.81	0.32	0.11	0.07	
1.50			0.41	3.75	4.30	2.43	1.44	1.23	0.61	0.24	0.08	0.04
1.75			0.05	1.23	2.55	1.59	0.86	0.67	0.42	0.24	0.10	0.03
2.00				0.72	3.32	2.39	1.34	0.74	0.71	0.33	0.06	0.04
2.25				0.12	1.56	1.68	0.87	0.42	0.27	0.16	0.04	0.02
2.50				0.03	1.32	2.17	1.09	0.52	0.27	0.24	0.08	0.04
2.75					0.30	1.07	0.65	0.33	0.13	0.13	0.07	0.03
3.00					0.16	1.05	1.14	0.38	0.13	0.11	0.09	0.05
3.25					0.05	0.39		0.23	0.05	0.09	0.06	0.03
3.50								0.37	0.10	0.06	0.05	0.04
3.75									0.08	0.03	0.02	0.01
4.00										0.04		
4.25												
4.50												
4.75												
5.00												
5.25												
5.50												

Figure 5.5: Head waves: Workability horizontal distance

Also for the horizontal distance workability in Figure 5.5, a similar result is found compared to the mooring line tension workability. Only for sea conditions around Hs = 3.25m and higher, the conditions are not workable. This indicates that the station-keeping system, i.e. the mooring lines, are able to keep the vessel within the maximum allowable offset from its setpoint for nearly all sea conditions.

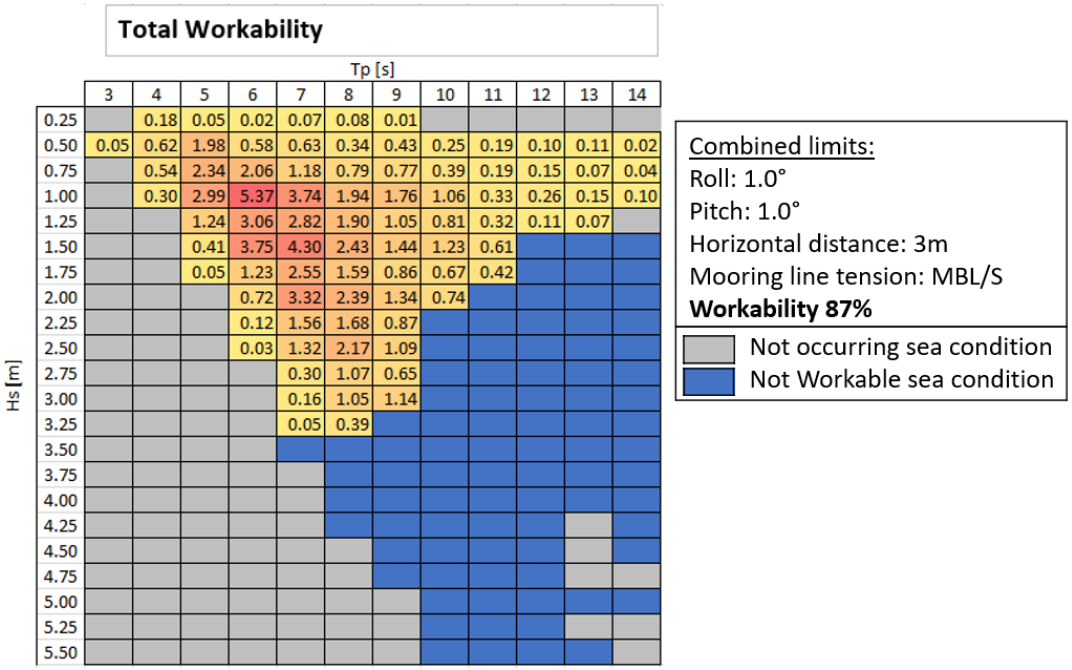

Figure 5.6: Head waves: Total Workability

The total workability of the installation is a combination of the workability from Figure 5.2 - 5.5. This means that a sea condition is found not workable if at least one of the mentioned limits is exceeded during an simulation. This total workability is mainly limited by the roll motions (Figure 5.2) and pitch motions (Figure 5.3) of the vessel.

5.4. Load case 2: Workability with gripper forces - 75 degrees

In Figures: 5.7 through 5.12 the calculated workability for Load case 2 is visualized.

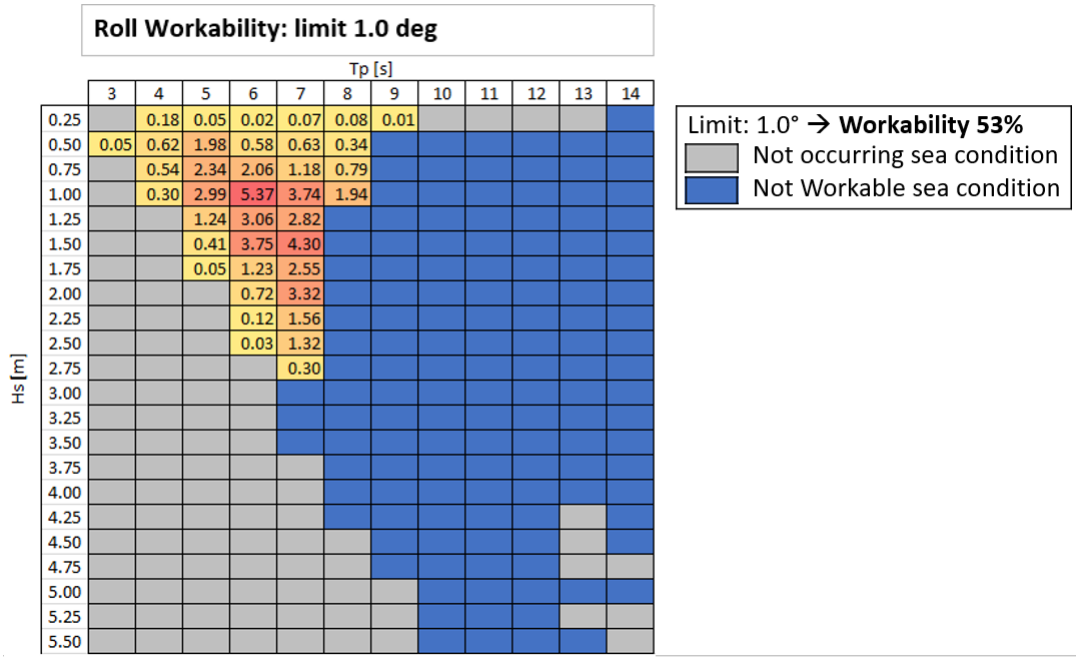

Figure 5.7: Beam waves: Workability roll

In Figure 5.7, the workability for roll is visualized. It can be seen that the roll motions become too

severe in sea conditions with a larger Tp. For $Tp \geq 8$s the roll motions increase significantly, even with a relatively low Hs. To show the significance of this increase in roll motions for larger Tp, the roll workability is visualized with a higher limit of 1.5 degrees. This can be seen in Figure 5.8.

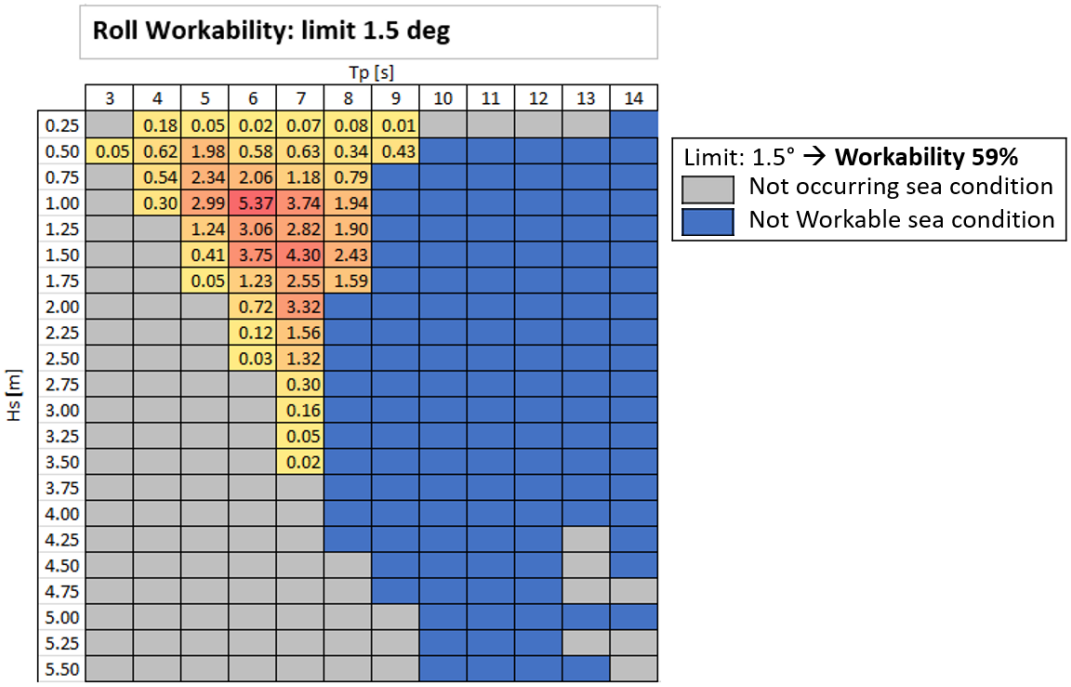

Hs [m] \ Tp [s]	3	4	5	6	7	8	9	10	11	12	13	14
0.25		0.18	0.05	0.02	0.07	0.08	0.01					
0.50	0.05	0.62	1.98	0.58	0.63	0.34	0.43					
0.75		0.54	2.34	2.06	1.18	0.79						
1.00		0.30	2.99	5.37	3.74	1.94						
1.25			1.24	3.06	2.82	1.90						
1.50			0.41	3.75	4.30	2.43						
1.75			0.05	1.23	2.55	1.59						
2.00				0.72	3.32							
2.25				0.12	1.56							
2.50				0.03	1.32							
2.75					0.30							
3.00					0.16							
3.25					0.05							
3.50					0.02							
3.75												
4.00												
4.25												
4.50												
4.75												
5.00												
5.25												
5.50												

Figure 5.8: Beam waves: Workability Roll - Limit 1.5 °

During the early driving phase of a monopile installation, the vibro drill is lifted on top of the monopile. During this lifting operation, the roll and pitch motions must remain below predefined limits to avoid swinging of the load. If the mass of the load is near the maximum crane lifting capacity, then the roll and pitch motions must be minimized i.e. the predefined roll and pitch motion limits are low (1.0 degrees). The mass of the vibro drill (1000 tonnes) is significantly heavy, but it is not near the maximum lifting capacity of the vessel (2000 tonnes). So, in practise, a vessel operator can decide to allow a higher roll motion limit of 1.5 degrees.

In Figure 5.8 it can be seen what the increase in workability is with a limit of 1.5 degrees (59%) compared to a limit of 1.0 degrees (53%). There is only a small increase in workability for a 1.5 degree limit compared to a 1.0 degree limit because the roll motions increase significantly at a larger Tp.

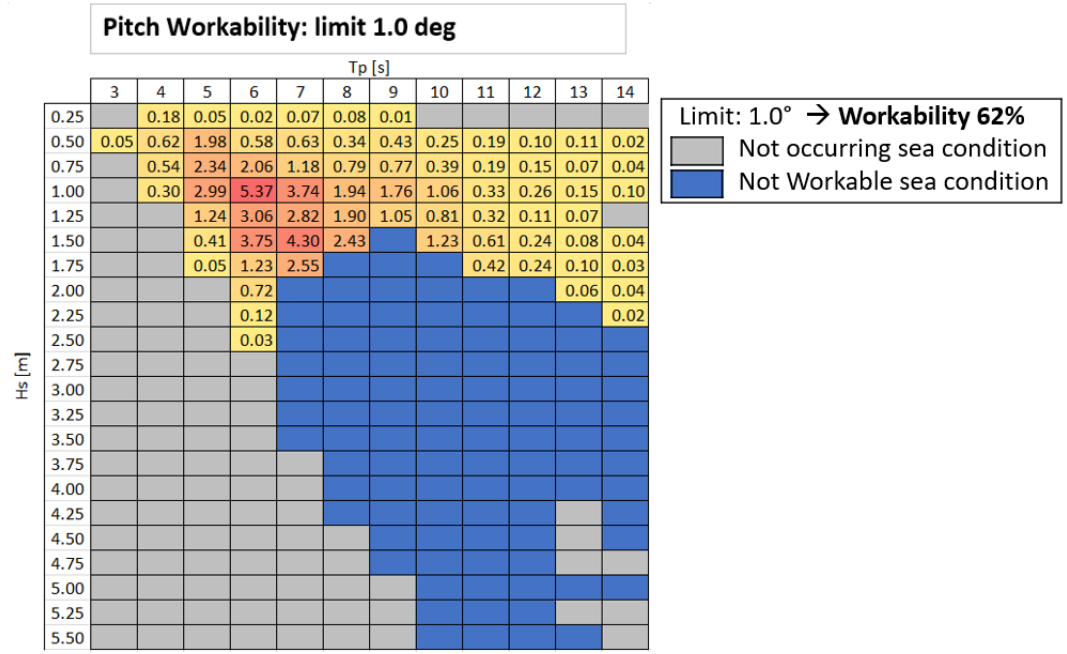

Hs [m] \ Tp [s]	3	4	5	6	7	8	9	10	11	12	13	14
0.25		0.18	0.05	0.02	0.07	0.08	0.01					
0.50	0.05	0.62	1.98	0.58	0.63	0.34	0.43	0.25	0.19	0.10	0.11	0.02
0.75		0.54	2.34	2.06	1.18	0.79	0.77	0.39	0.19	0.15	0.07	0.04
1.00		0.30	2.99	5.37	3.74	1.94	1.76	1.06	0.33	0.26	0.15	0.10
1.25			1.24	3.06	2.82	1.90	1.05	0.81	0.32	0.11	0.07	
1.50			0.41	3.75	4.30	2.43		1.23	0.61	0.24	0.08	0.04
1.75			0.05	1.23	2.55				0.42	0.24	0.10	0.03
2.00				0.72							0.06	0.04
2.25				0.12								0.02
2.50				0.03								
2.75												
3.00												
3.25												
3.50												
3.75												
4.00												
4.25												
4.50												
4.75												
5.00												
5.25												
5.50												

Figure 5.9: Beam waves: Workability pitch

Next, the pitch motions are visualized in Figure 5.9. These pitch motions are not particularly limited by a higher Tp. However, for $Hs \geq 1.75$, the pitch motions become too excessive at governing Tp values. For this reason, the workability is 62%.

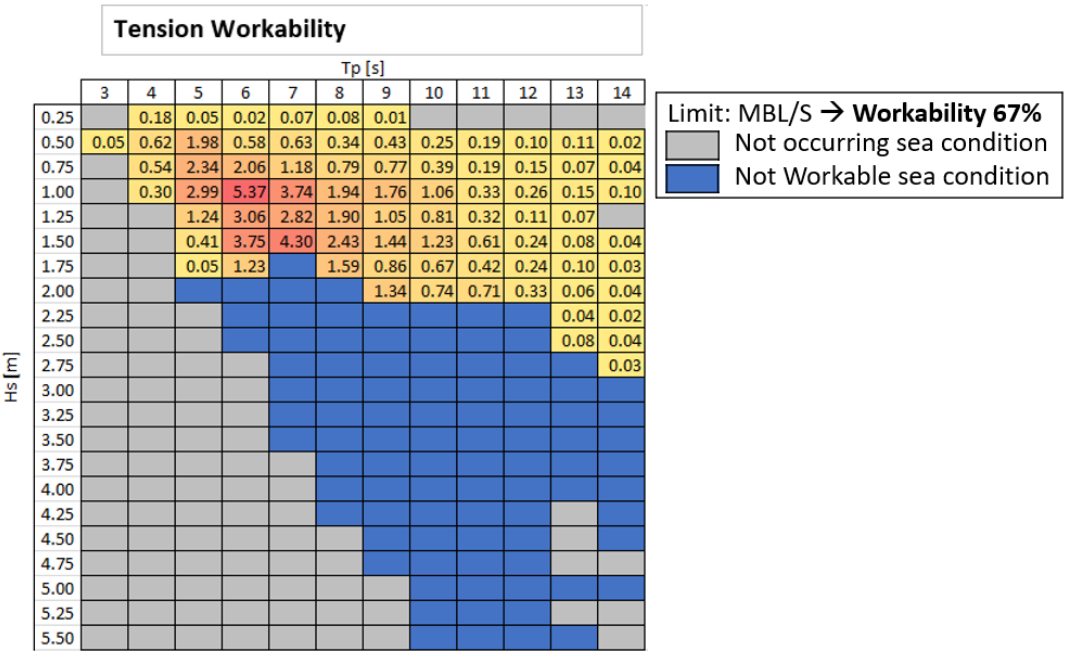

Hs [m] \ Tp [s]	3	4	5	6	7	8	9	10	11	12	13	14
0.25		0.18	0.05	0.02	0.07	0.08	0.01					
0.50	0.05	0.62	1.98	0.58	0.63	0.34	0.43	0.25	0.19	0.10	0.11	0.02
0.75		0.54	2.34	2.06	1.18	0.79	0.77	0.39	0.19	0.15	0.07	0.04
1.00		0.30	2.99	5.37	3.74	1.94	1.76	1.06	0.33	0.26	0.15	0.10
1.25			1.24	3.06	2.82	1.90	1.05	0.81	0.32	0.11	0.07	
1.50			0.41	3.75	4.30	2.43	1.44	1.23	0.61	0.24	0.08	0.04
1.75			0.05	1.23		1.59	0.86	0.67	0.42	0.24	0.10	0.03
2.00							1.34	0.74	0.71	0.33	0.06	0.04
2.25											0.04	0.02
2.50											0.08	0.04
2.75												0.03
3.00												
3.25												
3.50												
3.75												
4.00												
4.25												
4.50												
4.75												
5.00												
5.25												
5.50												

Figure 5.10: Beam waves: Workability Mooring line tension

The mooring line tension workability in Figure 5.10 shows a slightly higher workability compared to the pitch motion. The workability for mooring line tension is mainly limited by a larger Hs. For $Hs >$ 1.50 m, the tension in at least one of the mooring lines can become larger than the limit which is the minimum breaking load divided by the safety factor (MBL/S).

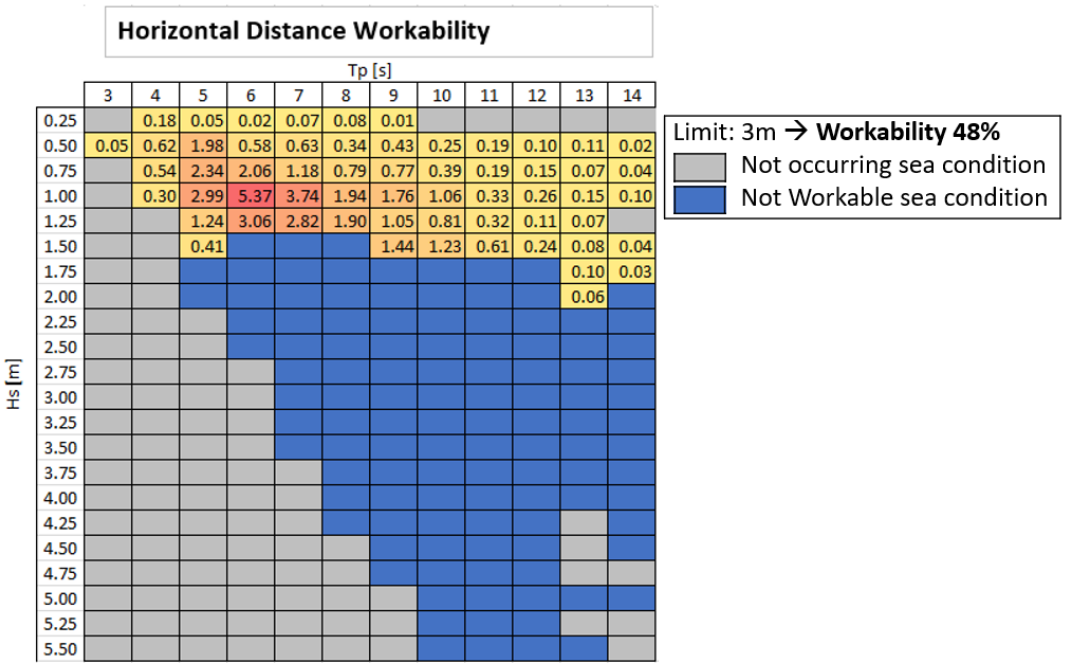

Figure 5.11: Beam waves: Workability horizontal distance

When the early driving phase has started, the monopile location in the horizontal frame is set and the vessel setpoint is determined. The task of the station-keeping system (the mooring lines in this case) is to keep the vessel as close as possible to this setpoint. The motion compensated gripper frame allows a drift (horizontal distance) from this setpoint until a maximum which is defined by the design of the gripper frame. In this research, that maximum drift is 3m.

The horizontal distance workability in Figure 5.11 shows a lower workability of 48% compared to the mooring line tension workability in Figure 5.10. This is mainly due to excessive motions at larger Hs. Above Hs = 1.25, the horizontal vessel motions become too excessive. This is because the vessel station-keeping system is not able to keep the vessel close enough to its setpoint.

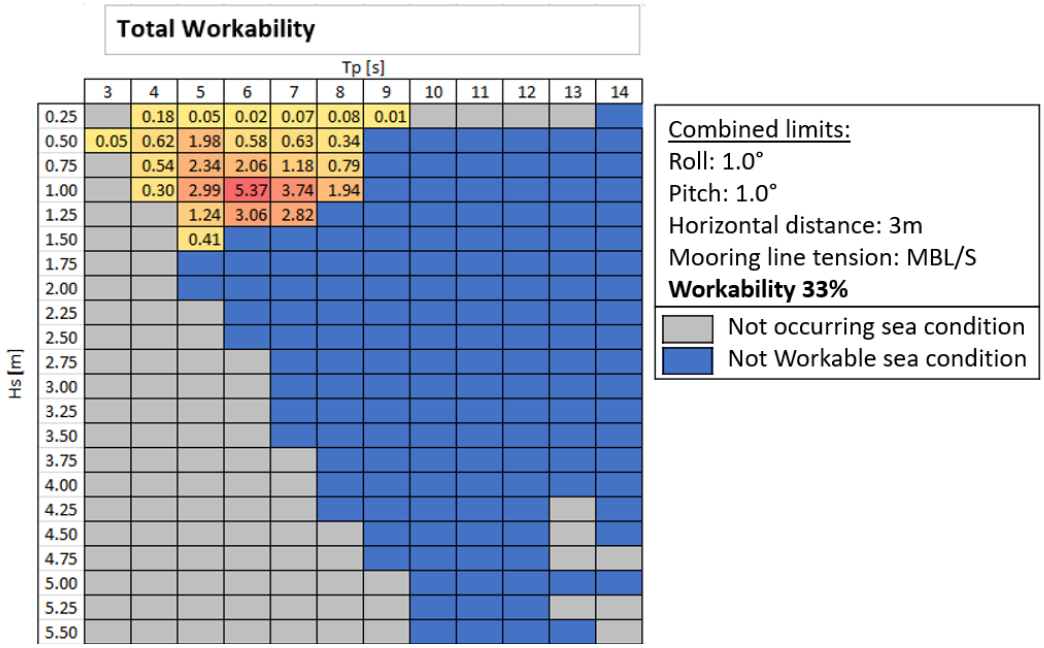

Figure 5.12: Beam waves: Total Workability

The resulting total workability of 33% is visualized in Figure 5.12. The workability is mainly limited by the roll motion (Figure 5.7) and the horizontal distance (Figure 5.11). The excessive roll motion at higher Tp limits the workability for $Tp \geq 8$s. Also, the total workability is limited by the horizontal distance motion at larger Hs.

5.5. Load case 3 and 4: Workability without gripper forces

This section shows how significant the influence of the gripper forces is on the total workability. Load cases 3 and 4 are identical to load cases 1 and 2 respectively except that forces from the gripper frame are not applied to the vessel in the simulations.

The results of Load case 3 and 4 show no significant differences from Load case 1 and 2 i.e. the workability Figures for Load case 3 and 4 are identical to Figures 5.2 through 5.12 from Load case 1 and 2.

6

Conclusions and recommendations

This chapter discusses the conclusions and limitations of this research and recommendations for future research are given.

6.1. Conclusions

The research question is:

"What is the workability of the early pile driving phase (phase 4) of a monopile installation with HLCV Stella Synergy using moorings as a station-keeping method and what is the influence of the gripper forces on this workability?"

To answer this question, a hydrodynamic database is derived from scale model test results. Viscous damping is added to this hydrodynamic database to realize a similar response as was measured in the scale model tests. It can be concluded that the provided hydrodynamic database showed very similar responses compared to the results from the model tests. Although the results of the model test and the hydrodynamic database are very similar, it is also found that the system responses are highly sensitive for variations in the added viscous damping.

To analyze the worst case scenario, a loading condition with a high GM value is analyzed. This loading condition is considered the most unfavorable in terms of roll motion due to its low natural roll period t_n= 12s. Around this period there is significant wave energy present for a large part of the wave conditions in the North Sea. This results in roll resonance during governing sea conditions causing the limits to be exceeded when the wave peak period Tp approaches the roll natural frequency. This is explicitly visible in the loading conditions with beam waves.

It is also found that the tested station-keeping system, i.e. the mooring lines, performs very unsatisfactory in beam waves. The mooring system is not able to maintain position within the envelope of the gripper for governing sea conditions. The mooring system is not able to maintain position for Hs > 1.25 in beam waves. This limits the total workability of the installation. Also, the tension in the mooring lines approaches the limit for Hs > 1.5 which is a wave height well below a condition that is deemed feasible in terms of workability.

A simplified monopile model is used to calculate the horizontal gripper forces during a monopile installation. The monopile, vibro drill and trapped water together are modeled with a hinge at the seabed. No monopile-soil interaction is assumed to study the worst case scenario during the early driving phase of a monopile installation. In the monopile model, only the resulting forces from the gripper frame are incorporated. The gripper frame controller used in this model does not incorporate dynamic pressure build-up in a hydraulic cylinder. Only instantaneous static forces are generated by the gripper frame controller. Incorporating this dynamic effect can have a significant influence of the gripper frame forces. Furthermore, the forces from the gripper frame are derived from an iteration. In this research, the generated gripper forces do not cause an increase in drift motion of the vessel.

In general, the total system performs unsatisfactory in beam waves, with a total workability of 33%. The total workability is limited by the roll motions and by the lack of station-keeping during the installation. The roll motions become too excessive for longer waves. In beam waves, the total drift forces on the vessel are larger compared to head waves for a monohull vessel such as HLCV Stella Synergy. Due to these large drift forces in beam waves, the drift motion of the vessel becomes larger than the limit of the gripper frame in sea conditions with Hs > 1.25m. In head waves, the total system performs satisfactory with a workability of 87%. This total workability is limited by the roll and pitch motions of the vessel. The station-keeping system is able to maintain position for sea conditions with $Hs \leq$ 3.0m.

6.2. Recommendations

The hydrodynamic database used in this thesis is based on the results of a model scale test for HLCV Stella Synergy. It is possible that the hydrodynamic properties of the vessel are different than the results of the model scale tests. This must be verified once the vessel is built. It is especially important to validate the added viscous roll damping coefficients for future studies because the system is highly sensitive for variations in these coefficients. Investigation is therefore needed for the determination of realistic viscous loads. Furthermore, the validity of the hydrodynamic properties is not guaranteed for other vessels.

The loading condition considered in this thesis, with a high GM value, is considered the worst case scenario in terms of roll motion due to its roll natural period. However, it is not investigated whether this high GM loading condition can actually occur during a monopile installation. It is advised to investigate what is exactly the most unfavorable loading condition that is likely to occur. Furthermore, the GM value changes when a load is lifted, because the CoG of the load is assumed to be at the crane tip. To obtain preferable loading conditions during a lifting operation, the GM value can be influenced by adding or removing ballast from the ballast tanks in the vessel hull. It is advised to avoid the loading condition with a high GM value. This means it is advised not to add too much ballast to the ballast tanks because then the total CoG is lowered (resulting in a high GM value).

The monopile model used in this research is a simplified mathematical representation of reality. The monopile-soil interaction and the hydrodynamic damping is neglected in this research. Only the trapped water is modeled as added mass. As an addition, the frequency dependent added mass and damping coefficients can be included in the model. This can influence the dynamic behavior of the monopile under environmental loading.

The gripper frame controller used in this thesis consists of a PID-controller. The monopile motions are fed into this controller. It is assumed that these monopile motions are known exactly while in reality, these motions are measured by motion sensors. A level of uncertainty is thus not modeled.

In this research, only one mooring line arrangement is tested. This mooring line arrangement consists of eight mooring lines which are deployed in the direction visualized in Figure 4.2. In beam waves, the vessel experiences high drift loads compared to head waves and the mooring lines are not able to maintain position sufficiently. For future studies it can be useful to change the mooring arrangement to obtain a better result. This can be done by adding more mooring lines, or by changing the direction in which the mooring are deployed.

The total system has an unfavorable workability in beam waves but proves to have a rather favorable workability in head waves. Unfortunately, weathervaning is not possible when the vessel is moored to the seabed. Although an installation on DP was not a subject in this research, it can prove to be a station-keeping method with a large workability due to the possibility to weathervane towards a most favorable incoming sea direction.

Only one installation phase is investigated in detail in this research. A different installation phase could prove to be more critical. For instance: Only a monopile penetration by self-weight is investigated. When the penetration depth increases, the monopile can start to exert mooring forces to the gripper frame which can influence the workability.

The wave scatter diagram used in this thesis is based on weather data from an entire year. There are seasonal differences in wave conditions that are not captured in this scatter diagram. There are some periods in a year where it is restricted to perform an offshore installation due to animal breeding seasons. It can be insightful to use wave data which does not include the animal breeding seasons

Only the wave conditions that are present in the North sea are addressed in this research. When other locations are investigated, a different approach is needed. In areas with a lot of swell, the waves can come from more than one direction. In this research the waves come from a single direction.

Bibliography

[1] L.G. Buitendijk. *Floating installation of offshore wind turbine foundations, Van Oord*. PhD thesis, Delft University of Technology, 2016.

[2] DNV-RP-C205. Environmental conditions and environmental testing. Technical Report October, DET NORSKE VERITAS, 1993.

[3] General Electric. World's Largest Offshore Wind Turbine | Haliade-X | GE Renewable Energy, 2019. URL https://www.ge.com/renewableenergy/wind-energy/offshore-wind/haliade-x-offshore-turbine.

[4] Jumbo. Jumbo Maritime, 2019. URL https://www.jumbomaritime.nl/.

[5] Jumbo Maritime. In-house knowledge, Menko Teunis, Marine Engineer, 2019.

[6] MacGregor. Combined expertise cuts wind turbine installation times - MacGregor.com, 2018. URL https://www.macgregor.com/news-insights/news-articles/2018/combined-expertise-cuts-wind-turbine-installation-times/.

[7] Pim Van Der Male. Offshore wind support structures. Technical Report November, Delft University of Technology, 2018.

[8] MARIN and Jumbo Maritime. Confidential Jumbo document - Model test report. Technical report, Jumbo Maritime, 2018.

[9] W.W. Massie and J.M.J. Journée. *OFFSHORE HYDROMECHANICS*. Delft University of Technology, first edition, 2001.

[10] Amir R. Nejad, Lin Li, Wilson Ivan Guachamin Acero, and Torgeir Moan. A systematic design approach of gripper's hydraulic system utilized in offshore wind turbine monopile installation. Technical report, Norwegian University of Science and Technology (NTNU), Madrid, 2018.

[11] North Sea Wind Power Hub. Modular Hub-and-Spoke concept to facilitate large scale offshore wind. Technical report, North Sea Wind Power Hub, 2019. URL https://northseawindpowerhub.eu/wp-content/uploads/2019/11/NSWPH-Drieluik-Herdruk_v01.pdf.

[12] Peutz. Condfidential Jumbo document: Wind load test report. Technical report, Jumbo Mariitme, 2018.

[13] Seajacks. Seajacks Scylla - Seajacks, 2018. URL http://www.seajacks.com/self-propelled-jack-up-vessels/seajacks-scylla/.

[14] Seaway Heavy Lifting. Seaway Heavy Lifting, 2015. URL https://www.seawayheavylifting.com.cy/.

[15] United Nations. Paris Agreement on Climate Change. In *Adoption of the Paris Agreement*, pages 11–22, 1992. doi: 10.1201/9781351116589-2.

[16] G A Van Der Veen. *Monopile upending workability and techniques*. PhD thesis, Delft University of Technology, 2019.

[17] WindEurope. Offshore wind in Europe, 2019. ISSN 14710846. URL https://windeurope.org/.

A

Specific information

A.1. HLCV Stella Synergy

Description	Symbol	Magnitude	Unit
Length between perpendiculars	L_{pp}		m
Breadth	B		m
Draught	T		m
Mass	m_{vessel}		mT
Displacement volume	∇		m^3
Mass radius of gyration around X-axis	K_{XX}		m
Mass radius of gyration around Y-axis	K_{yy}		m
Transverse metacentric height	GMt		m
Longitudinal metacentric height	GMt		m
Frontal area above waterline (surge direction)	A_F		m^2
Sideways area above waterline (sway direction)	A_S		m^2

Table A.1: HLCV Stella Synergy main specifications for the analyzed loading condition [MARIN and Jumbo Maritime, 2018]

A.2. Monopile

Description	Symbol	Magnitude	Unit
Total length	L_{mp}		m
External Diameter	D		m
Mass	m_{mp}		mT
Mass of trapped water	m_{tw}		mT
Water depth	d		m
Soil penetration depth	d_{pen}		m
Mass vibro drill	m_{vd}		mT
Height vibro drill	L_{vd}		m
Gripper height	L_{gp}		m

Table A.2: Monopile main specifications [Jumbo Maritime, 2019]

A.3. Gripper frame

Description	Magnitude	Unit
Maximum excursion from setpoint in x-direction		m
Maximum excursion from setpoint in y-direction		m
Maximum horizontal gripper force		kN
Position x relative to vessel COG		m
Position y relative to vessel COG		m

Table A.3: Gripper frame main specifications [Jumbo Maritime, 2019]

A.4. Mooring lines

The mooring lines consist of two sections. The first section, near the anchor, is a Chain. The second part is High Modulus PolyEthylene (HMPE) rope.

Description	Chain	HMPE	Unit
Section length	50		m
Diameter	76		mm
Weight in air	115		kg/m
Weight in water	100		
Axial stiffness	493270		kN
Minimum Breaking Load (MBL)	4294		kN
Safety Factor (S)	1.67		[-]

Table A.4: Mooring line main specifications [Jumbo Maritime, 2019]

B

Scatter diagram

Below the scatter diagram for the central North sea is depicted. The numbers resemble the probability of occurrence (%) of that particular combination of Hs and Tp.

Hs [m] \ Tp [s]	2 - 3	3 - 4	4 - 5	5 - 6	6 - 7	7 - 8	8 - 9	9 - 10	10 - 11	11 - 12	12 - 13	13 - 14	14 - 15	15 - 16	16 - 17	17 - 18	18 - 19	19 - 20
0.25		0.18	0.05	0.02	0.07	0.08	0.01					0.00						
0.50	0.05	0.62	1.98	0.58	0.63	0.34	0.43	0.25	0.19	0.10	0.11	0.02						
0.75	0.00	0.54	2.34	2.06	1.18	0.79	0.77	0.39	0.19	0.15	0.07	0.04						
1.00		0.30	2.99	5.37	3.74	1.94	1.76	1.06	0.33	0.26	0.15	0.10						
1.25		0.01	1.24	3.06	2.82	1.90	1.05	0.81	0.32	0.11	0.07	0.01						
1.50			0.41	3.75	4.30	2.43	1.44	1.23	0.61	0.24	0.08	0.04						
1.75			0.05	1.23	2.55	1.59	0.86	0.67	0.42	0.24	0.10	0.03						
2.00			0.01	0.72	3.32	2.39	1.34	0.74	0.71	0.33	0.06	0.04						
2.25				0.12	1.56	1.68	0.87	0.42	0.27	0.16	0.04	0.02						
2.50				0.03	1.32	2.17	1.09	0.52	0.27	0.24	0.08	0.04						
2.75					0.30	1.07	0.65	0.33	0.13	0.13	0.07	0.03						
3.00					0.16	1.05	1.14	0.38	0.13	0.11	0.09	0.05						
3.25					0.05	0.39	0.67	0.23	0.05	0.09	0.06	0.03						
3.50					0.02	0.22	0.84	0.37	0.10	0.06	0.05	0.04						
3.75						0.05	0.37	0.33	0.08	0.03	0.02	0.01						
4.00						0.02	0.33	0.39	0.12	0.04	0.03	0.02						
4.25						0.00	0.08	0.25	0.09	0.01		0.02						
4.50							0.05	0.29	0.14	0.04		0.01						
4.75							0.01	0.12	0.06	0.02								
5.00								0.15	0.09	0.04	0.00	0.01						
5.25								0.03	0.07	0.05								
5.50								0.04	0.12	0.05	0.00							
5.75																		
6.00																		

Figure B.1: Scatter diagram for the Central North Sea

C

Current and Wind coefficients

C.1. Current

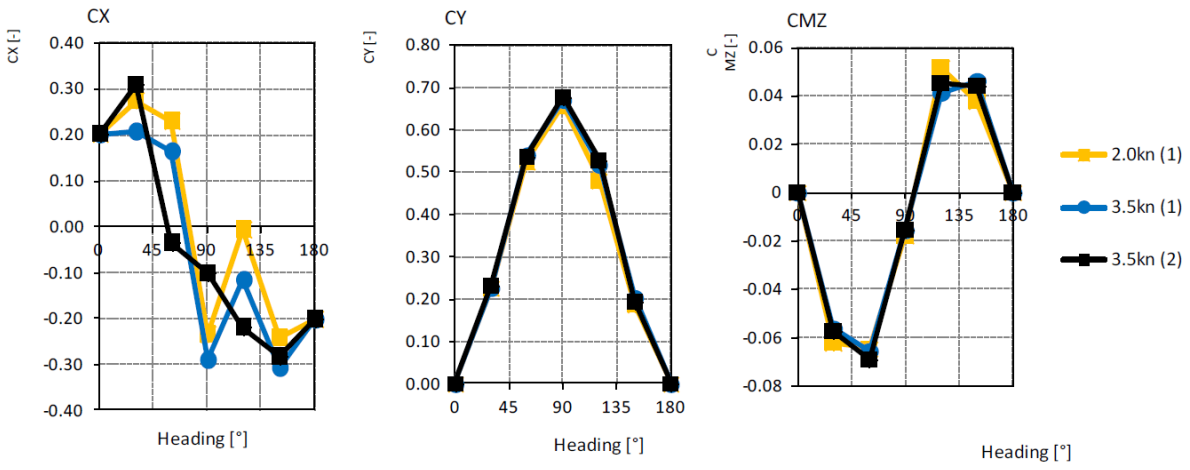

Figure C.1: Current coefficients HLCV Stella Synergy [MARIN and Jumbo Maritime, 2018]

C.2. Wind

Θ [°]	Cf_x	Cf_y	Cm_z
0	1.013	-0.003	0.01
15	1.01	0.156	0.012
30	1.024	0.374	-0.007
45	0.902	0.596	-0.017
60	0.595	0.795	-0.009
75	0.168	0.921	0.005
90	-0.118	0.985	0.029
105	-0.295	0.993	0.052
120	-0.459	0.932	0.071
135	-0.49	0.823	0.089
150	-0.661	0.596	0.079
165	-0.771	0.299	0.044
180	-0.732	0.032	-0.004
195	-0.758	-0.375	-0.065
210	-0.667	-0.671	-0.099
225	-0.543	-0.886	-0.106
240	-0.501	-0.979	-0.085
255	-0.325	-1.01	-0.054
270	-0.226	-1.01	-0.034
285	0.051	-0.939	-0.005
300	0.501	-0.823	0.019
315	0.862	-0.637	0.035
330	1.005	-0.423	0.033
345	1.03	-0.196	0.02

Figure C.2: Wind coefficients HLCV Stella Synergy [Peutz, 2018]